Development and Application of the Finite Difference Time Domain (FDTD) Method

by

Wei Fan

Submitted in partial fulfilment of the requirements
for the degree of Doctor of Philosophy

at

Dalhousie University
Halifax, Nova Scotia
November, 2017

I dedicate this thesis to my dear wife Xi Zhong for all her love, support, and always sharing her valuable thoughts with me.

Table of Contents

List of Tables

List of Figures

Abstract

Time-domain numerical methods are widely applied in modern engineering problems. In modeling electromagnetic structure problems, finite-difference time-domain (FDTD) method is one of the most well-known and widely adopted methods due to its algorithmic simplicity and flexibility. The major constraint of the FDTD method is, in its iterative solution process, that the time step is restricted by the Courant-Friedrichs-Lewy (CFL) condition. Simply to say, the finer the spatial discretization (often required by accuracy), the smaller time step that can be used. As a result, the computational speed and efficiency are limited. In the first half of this thesis, we analyze the FDTD method, review its instability and present its eigen-mode decomposition. Based on the finding, we then derived the analytic solution of the FDTD method, presenting an alternative non-iterative time-domain approach for electromagnetic problems. In the second half of the thesis, we focus on an important application of the FDTD method, the computational time reversal (TR) technique, which is an algorithm applied in inverse source problems such as source reconstruction. The algorithm is thoroughly investigated in theory, a new condition is presented for precise source reconstructions, and a mathematical model is developed to reformulate the time-reversal process in an optimization manner. Finally, band-limited fields or signals are incorporated into the model to make the time reversal method practical. Initial numerical experiments are conducted, and the results demonstrate the effectiveness and potentials of the proposed time-reversal method in source reconstructions and microwave structure synthesis in the future.

List of Abbreviations Used

FDTD	Finite Difference Time Domain
CFL	Courant-Friedrichs-Lewy
TLM	Transmission Line Matrix
MOR	Modal Order Reduction
TR	Time Reversal
RLS	Regularized Least Square
PML	Perfectly Matched Layer
ABC	Absorbing Boundary Condition

Acknowledgements

I would like to thank my supervisor, Dr. Zhizhang Chen for his constant guidance, encouragement, support and patience. His insightful advice is very helpful for me to build the path of the research. His humor makes those like pleasant journeys. His broad vision in the research helped me look at the problems and issues from a higher dimension. I am very glad to be his student and be influenced by his way of thinking.

I greatly appreciate the support and advice from my other committee members, Dr. Sergey Ponomarenko, Dr. William Phillips, and Dr. Puyan Mojabi of the University of Manitoba.

I want to thank Dr. Shunchuan Yang, Dr. Xiaoyan Zhang, Dr. Aidong Yang, Dr. Farid Jolani, Dr. Colin O'Flynn, Luyun Wang and Dachuan Sun, for all their valuable thoughts shared with me in our numerous discussions and daily chatting. I am also thankful to Wan Peng, Jiacheng Guo, Dr. Zhimeng Xu, and all other colleagues at Microwave and Wireless Laboratory and I am glad to have them aside.

My thanks also go to Nicole Smith, Dr. Jason Gu, and all the faculty and staff of Department of ECE, for their support, help and warm smiles.

Finally, my thanks to my family and my parents, for always being there for me.

CHAPTER 1 INTRODUCTION

1.1 PREFACE

This thesis mainly focuses on investigations on time-domain numerical methods of computational electromagnetics; it includes the development of the finite-difference time-domain (FDTD) method, and its application in inverse source problems. This chapter is to introduce the research background and review the state-of-the-art of FDTD method, as well as the motivations and objectives. The contributions and the organization of the thesis will also be presented.

1.2 RESEARCH BACKGROUND

Solutions of partial differential equations (PDEs) are much demanded for modern engineering problems. For example, Diffusion equation, Poisson equation, Laplace equation, Maxwell equations, and Schrödinger equation, are well-known PDEs that are widely studied and used in various fields. There are mainly two ways to solve PDE, analytic approach and numerical approach. The analytic approach is explicit and accurate; hence it is preferred whenever it is applicable. However, there are very rare cases in which the analytical solutions are obtainable. Usually an analytical solution is available only when the shapes, boundaries of a problem structure or domain are regular and simple. For most practical situations, the effort needed to reach the analytic solution is too prohibitive. In short, the analytic approach is limited and unachievable in solving practical problems.

The second way is to use numerical methods. In a numerical method, the first step is to discretize the problem in space and time, transfer the problem from a continuous model into a discrete one. By applying numerical approximations of the differential operators, the PDEs is transformed into discrete equations in the discrete domain. Then the solutions to the discrete equations are sought which are expected to the approximations to the analytic solutions to the original continuous PEDs.

Finite-difference time-domain (FDTD) method [1] is one of the most well-known numerical methods to solve PDEs involving time. For electromagnetic problems, it

combines the finite difference algorithm with the specific lattice/grid pattern introduced by Yee in 1966. It was further developed by Taflove who named it in 1980 [2]. Since then, applications and research interests in this method have exploded as can be seen in millions of publications directly related to FDTD [3-6] so far. In the past four decades, due to FDTD's simplicity, robustness, and explicitness, the range of applications of FDTD has been expanded over a very wide spectrum[6].

However, for the explicit time-domain method like FDTD method, the maximum time step is restricted by the Courant-Friedrichs-Lewy (CFL) condition [7], which is related to the smallest cell size in a discretized spatial domain. It is the major constraint of FDTD in its iterative solution process where the choice of time step is restricted. The finer the spatial discretization is (often required by accuracy), the smaller time step that has to be used. Hence, when multi-scale structures or geometry fine devices are to be modeled, discretized grid or cell size must be small to capture the detail of geometries; so does the time step. The restriction imposes a limit on computational speed and efficiency; sometimes it can make the computational time prohibitively long. If the CFL condition is not satisfied, solutions of the FDTD method (as well as the other explicit time-domain methods) will become unstable and diverge as the time marches, leading to numerical explosive results.

To address the stability issue, in recent years, a number of unconditionally stable schemes have been developed to remove the dependence of time step on space step in the FDTD method. For example, the alternatively-direction-implicit (ADI) FDTD method was developed [8-12]. With the implicitness, the size of the time step can be made independent of cell sizes. Therefore, an arbitrarily large time step can be used with the only constraint on the time step being modeling accuracy. Other implicit unconditionally stable FDTD methods have been developed too in the past decades; they include the locally-one-dimensional (LOD) FDTD methods [13-15], the multi-stage split FDTD (SFDTD) [16, 17] and Crank Nicolson (CN) FDTD methods [18-21]. All of these methods are implicit methods that mathematically require a system matrix solution.

To less extent of the removal of the stability condition, other methods have also been proposed to relax the stability condition and enlarge the time steps. A spatial filtering technique has been developed to extend the stability limit of the explicit FDTD

method [22-25] in electromagnetics. The time step is successfully extended beyond the CFL limit, while the filtering process requires intensive computation. The cause of the instability is investigated with the eigen matrix theory and an unconditional FDTD scheme is introduced by modifying the conventional FDTD leap-frog iterative process [6, 26]. In these methods, the iterative march-on-time procedures are required and the CFL conditions are inherently present in the FDTD model.

On the other hand, as one of the important applications of the FDTD method or time-domain numerical methods in general, computational time-reversal (TR) techniques have been studied for solutions of inverse source problems in acoustics, electromagnetics and other areas [27-31]. To understand TR process, consider a two-step procedure: first signals (or fields) emitted by sources are propagated, recorded at pre-selected output locations in a solution domain, which can be named as forward propagation; then in a backward propagation, the recorded signals are reversed in time and re-injected at the output locations into the problem domain. This procedure is the time reversal method. As long as the solution domain is reciprocal, these re-injected signals (or fields) experience the same propagation conditions (e.g. multipath, reflections, refractions) as the forward propagating signals, resulting in field focusing or peaks around the original source locations. Robust and simple to implement, the TR methods have drawn much attention of the inverse problem community. In computational electromagnetics, TR methods have been formulated and implemented using the Transmission Line Matrix (TLM) method [32-34], and the Finite Difference Time Domain (FDTD) method [35]. In spite of the progress of the recent years in the area, there are still major challenges and issues with the TR techniques developed so far for practical applications. For example, the source locating by peak identification may not work well in certain cases, especially when multiple sources exist; and the relevant theory has not been developed. Also, the signals of full-spectrum are mostly not available for the inverse operation and the TR process. All these limitations motivate us for the further development of the TR techniques as one of the major applications of the FDTD method or time domain numerical methods in general.

1.3 OBJECTIVES

The objective of the thesis is to find new paths and formulations for the FDTD method and the applications in light of the challenges and issues described in the previous section. As the result of my work, this thesis achieves the following specific objectives of limited scope:

1) perform detailed analysis of the conventional FDTD method and theorizes its stability problem from the aspect of a discrete system for a time-domain method;
2) overcome constraint of CFL limit and develop a wave-equation based unconditionally-stable scheme for the FDTD solutions;
3) derive the analytical form of the FDTD solution;
4) develop the theoretical model for the time reversal method;
5) derive a condition for precise source reconstructions without false results;
6) reformulate and develop the TR process into an optimization problem for effective source identifications and reconstructions; and
7) propose an extraction method for incorporating band-limited signals or responses into the TR process for practical applications.

1.4 CONTRIBUTIONS OF THIS THESIS

This thesis presents the analysis of the essentials of the FDTD method. By considering FDTD method as a discrete system with input and output, the stability issue of FDTD method is studied in a succinct manner. Based on the analysis, a peculiar new phenomenon is first observed and reported: the CFL condition may not always guarantee the stability of FDTD method (and other time-domain methods).

With the stability studies, the cause of numerical instability is identified. By removing the unstable modes contained in the FDTD solutions, an unconditionally stable wave-equation FDTD method is developed. Numerical experiments are conducted to verify the unconditional stability.

Analytic form of FDTD solutions is derived for the first time. Solution of a FDTD model of a structure at any time step can then be obtained directly without the iterative process like that of the conventional FDTD simulation. Details of the analytical FDTD

solution in different scenarios of hard sources, lossy medium, and non-uniform dielectric materials are discussed and verified. Treatment of more complex scenario like absorbing boundary conditions are also discussed and a pathway is provided for future studies.

The time reversal method is an important application of the finite-difference time-domain method to solve inverse source problems. In this thesis, detailed theoretical models and analysis of time reversal in both time-domain and frequency domain are presented for the first time. They show that the conventional TR focusing relies on peak identification sometimes fails. To address this, a new mathematical condition for reconstruction of multiple sources are developed. To apply the condition as a direct source location solver, a new method, the regularized least square technique, is formulated for the TR process; it can present the accurate identification of the numbers, locations and amplitudes of the sources.

Signals used in the TR method requires full-spectrum information so far. However, in practice, signal information is often band-limited. To overcome the problem, in this thesis, an extraction method that allows the incorporation of the band-limited signals or field responses into the TR method is developed. It makes the TR method practical and useful.

The above work, as a part of this thesis, has been published in [36-40] and another two papers are currently accepted for publication. As the first author in the papers listed below, this PhD candidate is responsible of the theoretic developments, numerical verifications, organizing and writing of these papers.

[1] W. Fan, Z. D. Chen, and S. Yang, “A wave equation based unconditionally stable explicit FDTD method,” in *Proc. 2015 IEEE MTT-S International Conference on Numerical Electromagnetic and Multiphysics Modeling and Optimization (NEMO)*, 2015.

[2] W. Fan, Z. Z. Chen, and S. C. Yang, "On the Analytical Solution of the FDTD Method," *IEEE Transactions on Microwave Theory and Techniques*, vol. 64, pp. 3370-3379, Nov 2016.

[3] W. Fan, Z. Chen and W. J. R. Hoefer, "Source Reconstruction From Wideband and Band-Limited Responses by FDTD Time Reversal and Regularized Least Squares," *IEEE Transactions on Microwave Theory and Techniques*, vol. 65, no. 12, pp. 4785-4793, Dec. 2017.

[4] W. Fan and Z. Chen, "A new time reversal method with extended source locating capability," In *Proc. 2017 IEEE MTT-S International Microwave Symposium (IMS)*, Honololu, HI, 2017, pp. 704-706.
[5] W. Fan and Z. Chen, "A condition for multiple source reconstructions with the time-reversal methods," In *Proc. 2016 IEEE MTT-S International Microwave Symposium (IMS)*, San Francisco, CA, 2016, pp. 1-4.

1.5 ORGANIZATION OF THIS THESIS

Chapter 2 presents the detailed analysis of the FDTD method. By applying the matrix theory and the z-transform, it reveals the root cause of the instability of the FDTD method. Based on the analysis, it is discovered that the CFL condition does not always ensure the stability of The FDTD method as proved by numerical experiments. Furthermore, an unconditionally stable wave-equation based iterative method for the FDTD solutions is proposed. Numerical experiments verify the unconditional stability and effectiveness of the proposed method.

Chapter 3 develops the analytic solution of the FDTD method. For the first time, the analytic form of FDTD solution is explicitly represented, which makes possible to directly obtain FDTD simulation results at any time given without the conventional iterative march-on-time process. The analytic solution is mathematically derived and numerically verified. Besides, notable cases such as hard source, lossy medium and non-uniform dielectric materials are considered and variants of the analytic solutions are also presented. Future directions of handling of absorbing boundary conditions are also provided.

Chapter 4 dedicates to the application of time-domain methods to the time reversal (TR) method. The TR technique is applied in solving the inverse source problems such as source reconstructions. However, the conventional time reversal method is limited in practical applications for possible false results. Detailed theoretical analysis of the time reversal in both temporal and frequency domain are presented for the first time. A new condition is developed for reconstruction of multiple sources with

removal of the possibility of the false results. A mathematical formulation is then developed for the TR process for precise source reconstructions. To make the TR process practical, an extraction method is developed that can expand the band-limited signals or field responses to the full-spectrum signals for incorporations into the TR process. These developments lay the foundations for making the TR method practical for source reconstructions and synthesis in the near future.

Chapter 5 concludes the research in the thesis and presents the future directions.

CHAPTER 2 THE STABILITY OF THE FDTD METHOD AND THE UNCONDITIONALLY-STABLE WAVE-EQUATION BASED METHOD

2.1 INTRODUCTION

Many numerical methods have been developed to solve Maxwell's equations for electromagnetic structure problems. Among them, the explicit time-domain numerical methods such as the FDTD method [1, 2], has attracted particular interest for their capability of modeling transient responses. Besides, the explicit methods are normally free of matrix solutions and their solutions reflect physical events in its natural temporal dimension, providing a wideband solution with a single run of simulation. It also has advantages in modeling nonlinear phenomenon without much difficulty.

However, for the explicit time-domain methods, the time step size is restricted by the Courant-Friedrichs-Lewy (CFL) condition [3, 7], which places an upper limit of the time step of these explicit numerical methods; it hence restricts computational speeds and efficiency. If a time step is chosen larger than the CFL limit, the time-domain solutions of these methods will become unstable and divergent as they march on time. The limit depends on the sizes of elements or grids which discretizes solutions domains and properties of the media to be modeled. The smaller the elements (or finer the numerical grids) are, the smaller the limit is. As a result, the CFL condition may cause long, sometimes prohibitively long, simulation time due to the small time step that has to be taken.

Extensive research efforts have been made recently in circumventing the CFL condition by developing implicit FDTD methods [8, 9, 11, 41] or relaxing or even removing the CFL-caused instability [26, 42]. For example, spatial filtering is used to remove unstable solutions by filtering out the higher-order components in spatial domain [23-25, 42].

In this chapter, we will show that the FDTD (and other time-domain methods) is a discrete system with singularity poles in its impulse response; the CFL condition only ensures that the position of the poles will not result in instability for the impulse response

but not necessarily the FDTD solutions at all the times. By applying the eigen matrix analyses, the poles are found to be related to the eigenvalues of the FDTD system matrix; and the instability is caused by the eigenvalues whose values are larger than 4. In addition, large eigenvalues and their corresponding eigenmodes are found to corresponds to high frequency components of the FDTD solutions. By removing the high-frequency eigenmodes that cause the instability, a wave-equation based FDTD solution is developed to solve electric and magnetic fields explicitly without numerical instability. The details are presented in the following sections.

2.2 MATRIX FORMULATION OF THE FDTD METHOD AND STABILITY ANALYSIS

2.2.1 The Matrix Formulation of The FDTD method

Consider Maxwell's equations in an isotropic and lossless medium of permittivity ε and permeability μ:

$$\begin{aligned} \nabla \times \mathbf{E} &= -\mu \frac{\partial \mathbf{H}}{\partial t} , \\ \nabla \times \mathbf{H} &= \varepsilon \frac{\partial \mathbf{E}}{\partial t} + \mathbf{J} , \end{aligned} \tag{2.1}$$

in which **E** represents the electric field, **H** represents the magnetic field. **J** is the electrical current. With replacements of the derivatives with their central finite difference counterparts, equation (2.1) is discretized in both space and time. The results are the march-on-in-time formulations of the FDTD method:

$$\mathbf{H}[n+\frac{1}{2}] = \mathbf{H}[n-\frac{1}{2}] - \Delta t \mathbf{D}_E \mathbf{E}[n] , \tag{2.2a}$$

$$\mathbf{E}[n+1] = \mathbf{E}[n] + \Delta t \mathbf{D}_H \mathbf{H}[n+\frac{1}{2}] - \frac{\Delta t}{\varepsilon} \mathbf{J}[n+\frac{1}{2}] . \tag{2.2b}$$

where Δt is the discretizing time step, $\mathbf{H}[n-\frac{1}{2}]$ is a column vector whose elements are magnetic field at all the magnetic field grid points (or nodes) at time instant

$t = (n - \frac{1}{2})\Delta t$, $\mathbf{E}[n]$is a column vector whose elements are electric field at all the electric field grid points at time instant $t = n\Delta t$, $\mathbf{D}_E$ is the matrix of dimension $N_h \times N_e$ representing the finite-difference form of operator $\mu^{-1}\nabla\times$ and $\mathbf{D}_H$ is the matrix of dimension $N_e \times N_h$ representing the finite-difference form of operator $\varepsilon^{-1}\nabla\times$. n is the time step stepping index, N_e is the number of the electric field nodes and N_h is the number of magnetic field nodes.

Eq. (2.2) is the leap-frog form of the conventional FDTD formulation. As can be seen, the electric and magnetic field are solved in an alternating manner half a step apart. Eq. (2.2) can be further simplified by substituting (2.2b) into (2.2a) and vice versa. The results are the discretized wave equations for electric or magnetic fields, respectively:

$$\mathbf{E}[n+1] + \mathbf{E}[n-1] - 2\mathbf{E}[n] + \Delta t^2 \mathbf{D}_H \mathbf{D}_E \mathbf{E}[n] = -\frac{\Delta t}{\varepsilon}\left(\mathbf{J}[n+\frac{1}{2}] - \mathbf{J}[n-\frac{1}{2}]\right), \quad (2.3a)$$

$$\mathbf{H}[n+\frac{3}{2}] + \mathbf{H}[n-\frac{1}{2}] - 2\mathbf{H}[n+\frac{1}{2}] + \Delta t^2 \mathbf{D}_E \mathbf{D}_H \mathbf{H}[n+\frac{1}{2}] = -\frac{\Delta t}{\varepsilon}\mathbf{D}_E \mathbf{J}[n+\frac{1}{2}] \ . \quad (2.3b)$$

The numbers of unknown quantities of (2.3a) and (2.3b) are N_e and N_h, respectively.

The above two equations have the similar form. Therefore, they have the same CFL condition, which is also the CFL condition of the FDTD formulation (2.2) (since (2.3) is derived from (2.2)). We take electric field wave equation (2.3a) for our analysis. It can be simply rewritten as

$$\mathbf{E}[n+1] + \mathbf{E}[n-1] - 2\mathbf{E}[n] + \mathbf{M}\mathbf{E}[n] = \mathbf{x}[n] \ \ (\text{input}) \ . \quad (2.4)$$

where $\mathbf{M} = \Delta t^2 \mathbf{D}_H \mathbf{D}_E$ which is the finite-difference form of operator $\Delta t^2 (\varepsilon\mu)^{-1}\nabla\times\nabla\times$. $\mathbf{x}[n] = -\varepsilon^{-1}\Delta t\left(\mathbf{J}[n+1/2] - \mathbf{J}[n-1/2]\right)$ which represents the source term. In the case of known boundary conditions, it may also include boundary condition terms imposed.

2.2.2 Eigen-Analysis of the FDTD Method

Denote the Matrix **M** as the system matrix of The FDTD method. It has a dimension of $N_e \times N_e$, N_e is the number of the electric field nodes. It is a real symmetric matrix as well as semi-positive definite [6, 26]. Therefore, its eigenvalues are non-negative real numbers and its eigenvectors are linearly independent of each other. As a result, N_e eigenvectors of **M** form a complete solution space for the FDTD electric field solutions. In other words, any FDTD electric field solutions can be represented by a combination of these eigenvectors.

Denote $\mathbf{\Lambda} = diag[\lambda_1 \ \lambda_2 \ ... \ \lambda_i \ ... \ \lambda_{N_e}]$as the eigenvalue matrix of **M** with its diagonal elements being the eigenvalues, $\mathbf{V} = [\mathrm{V}_1 \ \mathrm{V}_2 \ ... \ \mathrm{V}_i \ ... \ \mathrm{V}_{N_e}]$ as the associated eigenvector matrix of $N_e \times N_e$elements whose columns are eigenvector $\mathrm{V}_i$of $N_e \times 1$ elements that is associated with eigenvalue λ_i. We can then expand a FDTD field solution and its source at the *n*-th time step in terms of the eigenvectors as follows:

$$\mathbf{E}[n] = \mathbf{V}a[n] \tag{2.5a}$$

$$\mathbf{x}[n] = \mathbf{V}b[n] \tag{2.5b}$$

where $a[n] = [a_{1,n} \ a_{2,n} \ ... \ a_{i,n} \ ... \ a_{N_e,n}]^T$ and $b[n] = [b_{1,n} \ b_{2,n} \ ... \ b_{i,n} \ ... \ b_{N_e,n}]^T$ are the expansion coefficient column vectors at the *n*-th time step for $\mathbf{E}[n]$ and $\mathrm{x}[n]$; element $a_{i,n}$ and $b_{i,n}$ are the time-step dependent expansion coefficients.

Equation (2.5) indicates that any FDTD solutions and their sources can be expanded in terms of the spatially invariant eigenmodes with time-dependent expansion coefficients. Substitution of (2.5) into (2.4) leads to:

$$\mathbf{V}a[n+1] + \mathbf{V}a[n-1] - 2\mathbf{V}a[n] + \mathbf{M}\mathbf{V}a[n] = \mathbf{V}b[n] \ . \tag{2.6}$$

Since $\mathbf{MV}=\mathbf{V}\boldsymbol{\Lambda}$,

$$\mathbf{V}a[n+1]+\mathbf{V}a[n-1]-2\mathbf{V}a[n]+\mathbf{V}\boldsymbol{\Lambda}a[n]=\mathbf{V}b[n]\ . \tag{2.7}$$

By left-multiplying $\mathbf{V}^{-1}$ to both sides of (2.7), we obtain

$$a[n+1]+a[n-1]-2a[n]+\boldsymbol{\Lambda}a[n]=b[n]\ . \tag{2.8}$$

Since $\boldsymbol{\Lambda}$ is a diagonal matrix, equation (2.8) can be fully decomposed for every element $a_{i,n}$ of vector $a[n]$:

$$a_{i,n+1}+a_{i,n-1}-(2-\lambda_i)a_{i,n}=b_{i,n},\ \text{for } n=1,\,2,\,3,\,\ldots. \tag{2.9}$$

where n represents the n-th time step of the FDTD march on time.

From (2.9), we can see that the solution of the FDTD method can be decomposed in terms of eigen spatial eigenmodes with expansion coefficients $a_{i,n}$. If expansion coefficient $a_{i,n}$ diverges as n (or time) increases, the corresponding eigenmode, as a part of the FDTD solution, will diverge and make the FDTD solution divergent and unstable. Note that the eigenvector or eigenmodes are invariant with time, while the eigenvalues have a proportional relationship with the square of the time step chosen. In the following section, we will find how the eigenvalues influence expansion coefficients and eigenmodes and hence the stability of the FDTD solutions.

2.2.3 Stability Analysis of The FDTD Method

Eq. (2.9) can be considered as a series of discrete scalar sub-systems that can be solved recursively. Such discrete sub-systems can then be analyzed effectively with the Z-transform [43].

For simplicity and without loss of generality, it is assumed that the initial conditions are $a_{i,-n} = a_{i,0} = a_{i,1} = 0$ and they are applied henceforth. By applying the unilateral Z-transformation to both sides of (2.9), the following equations are obtained:

$$\begin{aligned} &zA_i[z] + z^{-1}A_i[z] - 2A_i[z] + \lambda_i A_i[z] = B_i[z] \ , \\ &H_i[z] = \frac{A_i[z]}{B_i[z]} = \frac{z}{z^2 + 1 - (2 - \lambda_i)z}, \end{aligned} \tag{2.10}$$

where $A_i[z] = Z\{a_{i,n}\}$ can be considered as the response or output function, $B_i[z] = Z\{b_{i,n}\}$ can be considered as the source or input function. $H_i[z]$ is then the transfer function (as used in the circuit theory) or impulse response (as referred in communications theory) in the Z-domain; the latter name of impulse response is used henceforth in this thesis.

Equation (2.10) has two poles which make its denominator zero. Denote these poles as z_{i1} and z_{i2}. The time-domain impulse response is the inverse Z-transform of (2.10):

$$h_i[n] = Z^{-1}\{H_i(z)\} \quad . \tag{2.11}$$

The two poles of discrete system described in (2.9), z_{i1} and z_{i2}, determines whether $h_i[n]$ will diverge or not and hence the stability of the FDTD system itself. Figure 2. shows the four scenarios where z_{i1} and z_{i2} are located differently and they are analyzed below.

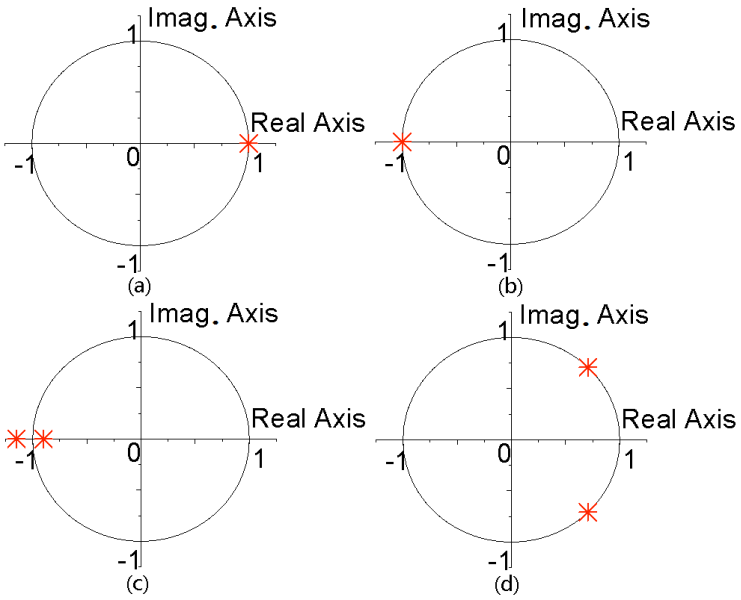

Figure 2.1 The four possible location scenarios of pole z_{i1} and z_{i2}

Scenario I (Figure 2.a): $z_{i,1} = z_{i,2} = 1$ (or $\lambda_i = 0$)

Equation (2.10) becomes:

$$H_i[z] = \frac{z}{(z-1)^2} \quad . \tag{2.12}$$

The corresponding impulse response is:

$$h_i[n] = n - 1 \quad \text{with } h_i[0] = h_i[1] = 0 \quad . \tag{2.13}$$

It means that the impulse response of the FDTD discrete system is increasing linearly with time in magnitude and hence is unstable. Note that (2.13) can be proven to be a solution of (2.9) by directing substituting it into (2.9) although (2.13) is a divergent solution in time.

Scenario II (Figure 2.b): $z_{i,1} = z_{i,2} = -1 (\lambda_i = 4)$

Equation (2.10) is then:

$$H_i[z] = \frac{z}{(z+1)^2} \quad . \tag{2.14}$$

Correspondingly the impulse response is

$$h_i[n] = (-1)^{n-1}(n-1) \quad \text{with } h_i[0] = h_i[1] = 0 \quad . \tag{2.15}$$

It means that the solution of the FDTD discrete system is oscillatory but increasing in magnitude linearly with time and hence is unstable.

Scenario III (Figure 2.c): $|z_{i,1}| > 1.0$ and $|z_{i,2}| < 1.0$ (or $\lambda_i > 4.0$)

Equation (2.10) has one pole $z_{i,1}$ lying outside the unit circle and another one $z_{i,2}$ inside the unit circle. The inverse of (2.10) presents the time-domain impulse response:

$$h_i[n] = \frac{1}{(z_{i,1} - z_{i,2})}(z_{i,1})^{n-1} + \frac{1}{(z_{i,2} - z_{i,1})}(z_{i,2})^{n-1} \tag{2.16}$$

with $h_i[0] = h_i[1] = 0$,

$$z_{i,1} = -\frac{\lambda_i - 2 + \sqrt{\lambda_i^2 - 4\lambda_i}}{2} = \frac{\lambda_i - 2 + \sqrt{\lambda_i^2 - 4\lambda_i}}{2} e^{j\pi} \tag{2.17a}$$

$$z_{i,2} = \frac{1}{z_{i,1}} = \frac{\lambda_i - 2 - \sqrt{\lambda_i^2 - 4\lambda_i}}{2} e^{j\pi} \tag{2.17b}$$

Since $|z_{i,1}| = \left|\frac{\lambda_i - 2 + \sqrt{\lambda_i^2 - 4\lambda_i}}{2}\right| > 1.0$, the impulse response (2.16) is divergent and the FDTD method is unstable.

By carefully examining the temporal frequencies of the poles, we have:

$$f_{i,1} = \frac{\pi}{2\pi\Delta t} = \frac{1}{2\Delta t} = \frac{f_s}{2}. \tag{2.18}$$

with $f_s = \frac{1}{\Delta t}$ being the temporal sampling frequency of the FDTD system. In other words, the poles that cause the instability carries a frequency that is one half of the FDTD sampling frequency.

Further mathematical analysis shows that $\lambda_i > 4.0$ corresponds to the case where the CFL condition is not satisfied (see Appendix I).

Scenario IV (Figure 2.d): $|z_{i,1}|=|z_{i,2}|=1.0$ (or $0<\lambda_i<4.0$)

Fig. 2.1d shows the positions of the two poles, z_{i1} and z_{i2}; they are conjugate to each other and are on the unit circle.

The impulse response can still be represented by (2.16) but the two conjugate poles are:

$$z_{i1,2}=e^{j\theta_{i1,2}}=\frac{(2-\lambda_i)\pm j\sqrt{4\lambda_i-\lambda_i^2}}{2} \tag{2.19a}$$

in which the angles are

$$\theta_{i1}=\arctan\left(\frac{\sqrt{4\lambda_i-\lambda_i^2}}{2-\lambda_i}\right)\ , \tag{2.19b}$$

$$\theta_{i2}=-\theta_{i1}\quad .$$

Analysis in Appendix I shows that it corresponds to the case where the CFL condition is satisfied. Mathematically, it means that the FDTD system is stable since $|z_{i,1}|=|z_{i,2}|=1.0$.

To further explore the relationships between the poles and the eigenvalues, Figure 2.2 and Figure 2.3 plot the relationships of poles and corresponding eigenvalues, showing the poles' magnitudes(largest of the two) and angles as function of the eigenvalues. The angle of the pole is equivalent to the angular frequency of the eigenmode.

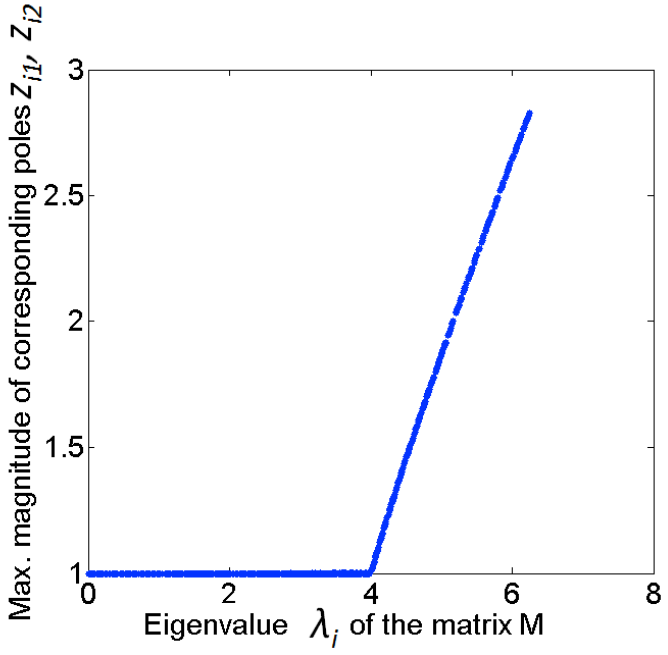

Figure 2.2 Largest magnitude of the two poles z_{i1} and z_{i2} versus the corresponding eigen value

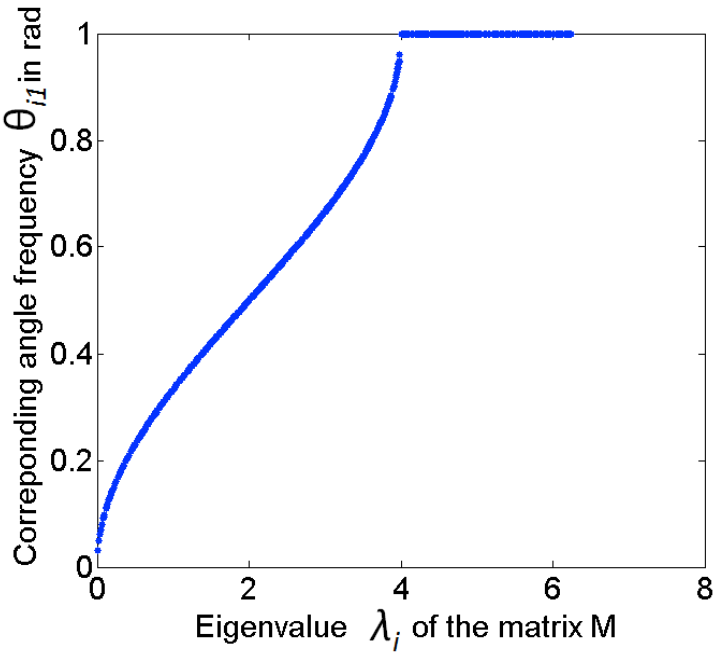

Figure 2.3 Angular frequency θ_{i1} of the eigenmode versus the eigen value λ_i

It can be seen that λ_i=4 is the cut-off point for both the two figures. From Figure 2.2, the largest magnitude of the two poles will be kept at 1 when the eigenvalue is smaller than 4. With eigenvalue larger than 4, the largest magnitude of pole will be over 1.

Instability occurs in such a case. In Figure 2.3, it reveals that the frequency of the eigenmode also has a monotonic mapping relationship when its eigenvalue smaller than 4. Larger eigenvalue corresponds to higher frequency, and vice versa. When the eigenvalue is larger than 4, the angular frequency of the eigenmode will equal to π.

In summary of the above four scenarios, it can be seen that the eigenvalue of the FDTD system matrix essentially determines the stability. The FDTD solution can be stable only if all the eigenvalues (or the maximum eigenvalue) of **M** satisfies:

$$\lambda_{\max}(\mathbf{M}) < 4 \tag{2.20}$$

In Appendix I, it is proven that the CFL condition is a necessary condition of (2.20) and thus the numerical stability of the FDTD model itself is ensured. Moreover, the eigenvalue also determines the temporal frequency of the corresponding eigenmodes. Eigenmodes with larger eigenvalue are of higher frequency in the FDTD solution, while the eigenmodes with smaller eigenvalue represents the low-frequency components. Since the instability is caused by the eigenvalues which are larger than 4, one can say that the FDTD instability is caused by high-frequency eigenmodes of the FDTD solution.

The above finding is very important. In practice, the spatial and temporal discretization in The FDTD method result in numerical dispersion [44, 45]. It means that the actual high frequent components of electromagnetic fields cannot be accurately modelled by the FDTD method. In other words, the high frequency components of the FDTD models represent numerical artifacts rather than its physical events. Therefore, removal of these high-frequency components in a FDTD model is not harmful to the accuracy of the FDTD solution. Based on this fact, we will propose an unconditionally stable wave-equation based FDTD method in section 2.5.

Although $0 <= \lambda_i <= 4$ can make the FDTD system stable, it is only the necessary condition not sufficient. In the following subsection, a further investigation is conducted.

2.3 An Exception: Can the CFL Condition Always Guarantees the Stability?

2.3.1 Theoretical Analysis

In this section, we focus the discussion on the scenario IV of section 2.3.2 where $0<\lambda_i<4$. As Fig. 2.1d shows, the FDTD discrete system have two conjugate poles on the unit circle, z_{i1} and z_{i2}, corresponding to the *i*-th eigenmode. The impulse response of the *i*-th eigenmode in the z-domain can be expressed as

$$H_i[z] = \frac{z}{(z - z_{i1})(z - z_{i2})} \tag{2.21}$$

The angles of the two poles are functions of the corresponding eigenvalue λ_i

$$\begin{aligned} \theta_{i1} &= \arctan\left(\frac{\sqrt{4\lambda_i - \lambda_i^2}}{2 - \lambda_i}\right) \\ \theta_{i2} &= 2\pi - \theta_{i1} \end{aligned} \tag{2.22}$$

As discussed in the previous section, the scenario corresponds to the case of a lossless FDTD system with the CFL condition satisfied. As conventionally believed, the FDTD solution will be stable.

However, we have discovered that in such a case, the FDTD system may not be stable when certain input is chosen. Consider a monochromatic input $x[n] = \cos[n\theta_{i1}]$. Notice that the angle frequency of the input coincides with one of the pole angle of the FDTD system. The z-domain interpretation of the source input is:

$$\begin{aligned} X[z] &= Z(x[n]) \\ &= Z(\cos[n\theta_{i1}]) \\ &= \frac{z(z - \cos\theta_{i1})}{z^2 - 2z\cos\theta_{i1} + 1} \\ &= \frac{z(z - \cos\theta_{i1})}{(z - \cos\theta_{i1} - j\sin\theta_{i1})(z - \cos\theta_{i1} + j\sin\theta_{i1})} \\ &= \frac{z(z - \cos\theta_{i1})}{(z - z_{i1})(z - z_{i2})} \end{aligned} \tag{2.23}$$

The output *y*[*n*] of (2.21) for the FDTD solution is then:

$$
\begin{aligned}
y[n] &= Z^{-1}(Y[Z]) = Z^{-1}(X[Z]H(Z)) \\
&= Z^{-1}\left(\frac{z^2(z-\cos\theta_{i1})}{(z-z_{i1})^2(z-z_{i2})^2}\right) \\
&= Z^{-1}\left(\frac{A_1}{(z-z_{i1})}+\frac{A_2}{(z-z_{i2})}+\frac{A_3}{(z-z_{i1})^2}+\frac{A_4}{(z-z_{i2})^2}\right) \\
&= A_1(z_{i1})^n + A_2(z_{i2})^n + A_3 n(z_{i1})^n + A_4 n(z_{i2})^n
\end{aligned}
\tag{2.24}
$$

Note that last two terms are multiplication of oscillation term $(z_{i1})^n$ and linearly-increasing term n. The term n will then lead to the uncontrolled increase output as time marches (or n increases). In other words, monochromatic input at specific angular frequencies will result in a second-order pole of the output in the Z-domain, causing the output to be divergent and unstable. More generally, any input, whose Z-domain expression has a pole coincides with any pole of the FDTD system will result in unstable FDTD solutions.

Since the angular frequency θ_{i1} is determined by eigenvalue λ_i of the FDTD system matrix **M** as shown in (2.22), the frequencies causing unstable FDTD solutions are eventually determined by the FDTD system.

In summary, the CFL condition, if satisfied, only guarantees the FDTD system itself is stable. The FDTD solutions are also dependent on the input or the excitations. If the excitations or the inputs contain components whose frequencies coincide with the eigen frequencies of the FDTD system, it is still possible to generate divergent FDTD solutions. To the author's best knowledge, this phenomenon has not been reported so far.

2.3.2 Verification of The Predicted Phenomenon

In the above section, an unreported case where the CFL condition doesn't guarantee the stable FDTD solution is shown. To verify this, a simple but typical numerical example is considered: a two-dimensional square cavity with the perfect conducting (PEC) boundary. It is simulated with the FDTD method.

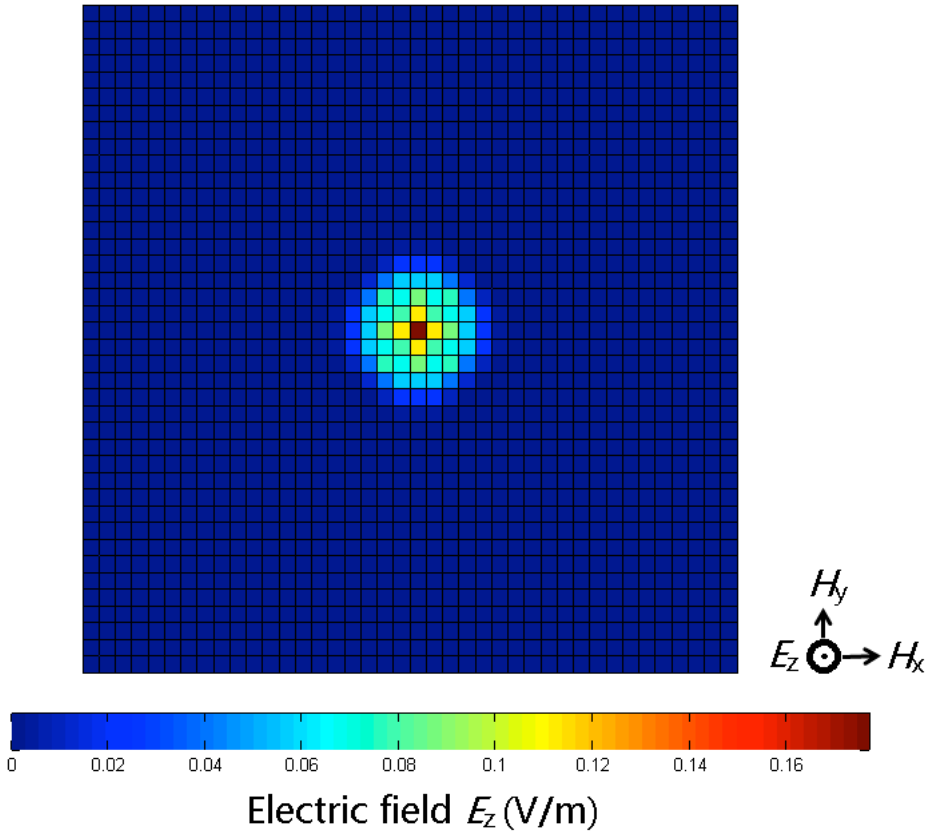

Figure 2.4. The square cavity with PEC boundary, TM wave excited.

A 41x41 evenly-spaced grid is used to discretize the cavity. The number of unknown electric field points is then 1521. The matrix **M** and its eigenvalues and eigenvectors can be obtained using eigen-solvers of various mathematical software packages. A point electric field source is put inside the problem area, here chosen to be at the centre, exciting a monochromatic sinusoidal signal into the space. The signal can be described as

$$\begin{aligned} \sin[n\theta] &= \sin[n(2\pi f \Delta t)] \\ \theta &= 2\pi f \Delta t \end{aligned} \tag{2.25}$$

The angle frequency is chosen equal to

$$\theta = \arctan \frac{\sqrt{4\lambda_i - \lambda_i^2}}{2 - \lambda_i} \tag{2.26}$$

in which the λ_i is one of the eigenvalue of the FDTD system matrix. By this source setting, the input will generate poles in Z-domain, who will coincide with the poles of the FDTD system.

The simulation is performed for 20000 steps. The recorded time-domain field values diverge as shown in Fig. 2.5;

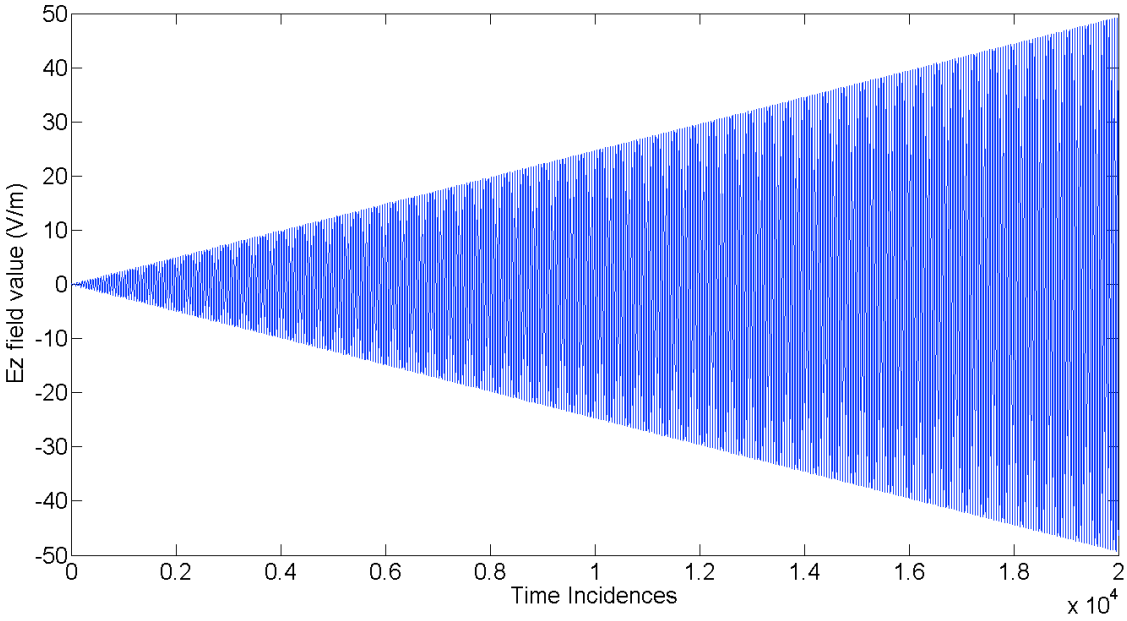

Figure 2.5 The time-domain electric field recorded at the center of the cavity for 20000 simulation time steps.

Although Fig. 2.5 shows the solution explosion, one may still question whether it is the result of the instability as previously described since the cavity is lossless and monochromatic signal is continuously injected into the FDTD computational domain. Another suspicion is that the diverging time-domain solution may be caused by the natural resonances of the cavity which can produce large field values. In the following paragraphs, we will address the concerns by carrying various numerical experiments.

More specifically, different angle frequencies are chosen for the monochromatic sources to excite the FDTD numerical grids. The frequencies are chosen from as follows, respectively:

(1) 0, which is a DC source;

(2) A random value between 0 and $f_s/2$, where $f_s = 1/\Delta t$ is the temporal sampling frequency;

(3) the natural resonant frequencies of the cavity calculated by (2.27)

$$f_c = \frac{1}{2\pi\sqrt{\mu\varepsilon}}\sqrt{\left(\frac{m\pi}{a}\right)^2 + \left(\frac{n\pi}{b}\right)^2} \quad ; \qquad \theta_c = 2\pi\Delta t f_c = \frac{\Delta t}{\sqrt{\mu\varepsilon}}\sqrt{\left(\frac{m\pi}{a}\right)^2 + \left(\frac{n\pi}{b}\right)^2} \tag{2.27}$$

in which a and b are the sizes of the cavity, respectively. m and n represent the mode indices of the TM(m,n) mode; and

(4) the unstable frequencies predicted by (2.26)

With each of the above four sources, FDTD simulation is performed over 50000 time steps. Maximum time-domain electric field values are recorded for each case. Figure 2.6 shows the results.

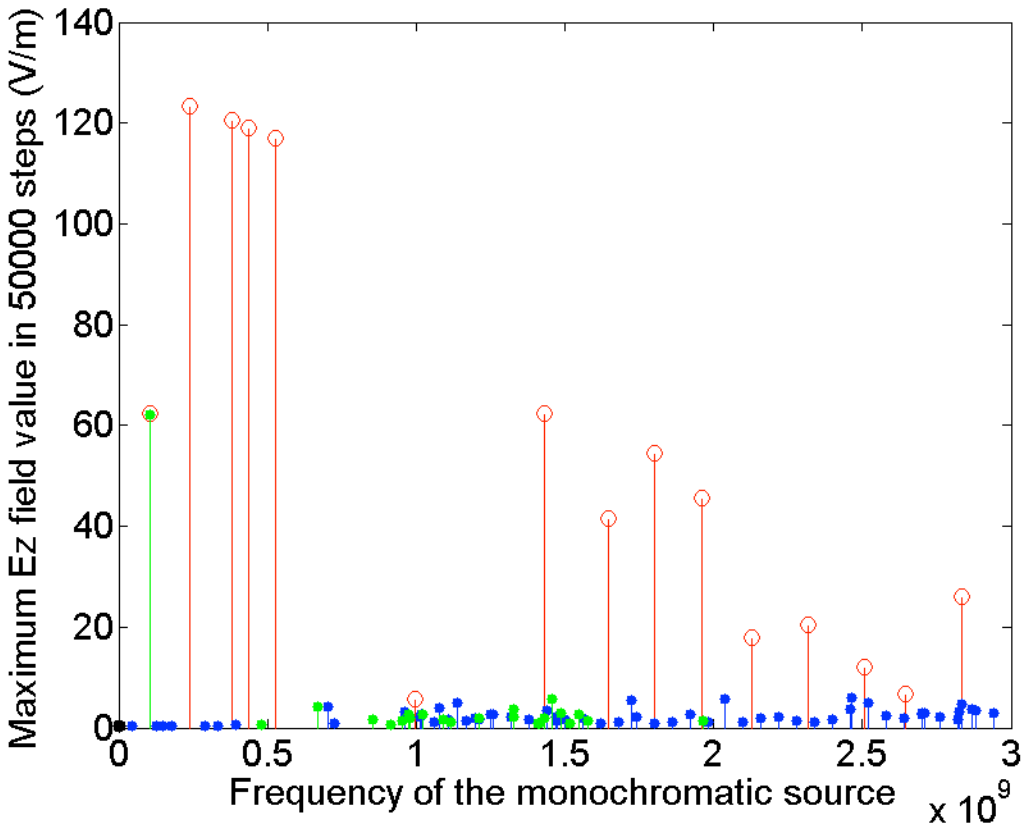

Figure 2.6 Maximum time-domain field value obtained within the 50000 steps of the simulations using monochromatic sources of different frequencies. Black dots are the results for case (1) (the DC source), blue dots for case (2) (a random frequency between 0 and $f_s/2$), green dots are for case (3) (a natural resonant frequency of the cavity), red circles for case (4) (the predicted unstable frequencies calculated by (2.26)).

It can be seen from Figure 2.6 the only in case (4), abnormally high values of electric field are observed, which indicates the instability of FDTD simulation occurs. As described above, these frequencies leading to unstable time-domain field solutions are just the unstable frequencies determined by eigenvalues of **M** through (2.26). Other frequencies, including the natural resonant frequencies of the cavity, do not introduce uncontrollable large field values (or numerical instability) in the tests, unless they happen to coincide with the unstable frequencies ash shown for case (4). This experiment shows that the abnormally high values are neither resulted from continuous monochromic signals nor natural resonances of the cavity; they came from the numerical instability discussed before.

Another interesting experiment is to test how sensitive the system is to the course frequency when it gets close to the unstable frequencies. By injecting monochromatic sources whose frequency is near the unstable frequency, maximum time-domain electrical field values over 20000 simulation steps recorded and shown below in Fig. 2.7. As the frequency approaches the unstable frequency, field value becomes larger and larger, eventually reaching uncontrollable high numbers; the instability occurs.

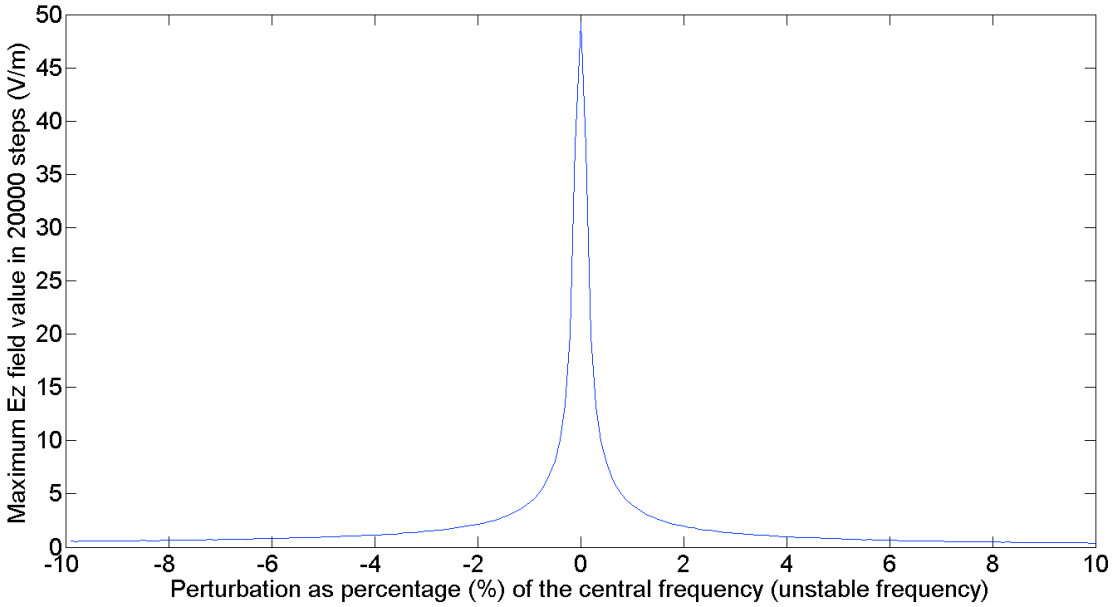

Figure 2.7 Maximum field values obtained with monochromatic sources whose frequencies are near an unstable frequency.

From Figure 2.7, it can be seen that if the source frequency is 2% off the unstable frequency, the FDTD solutions are normal without the instability issue. As a result, when the instability occurs when the CFL condition is satisfied, the source frequency needs to be moved away from the unstable frequency by more than 2%.

2.3.3 Discussions and Summaries

From the above analyses, we can have the following conclusions:

1) The FDTD solutions may be considered as consisting of many eigenmodes, the size of Matrix **M**, i.e. the number of unknown electric field nodes to be solved for.

2) The eigenvalues associated with the eigenmodes are proportional to the square of the FDTD time steps. When the eigenvalue is smaller than or equal to 4, the associated eigenmode is stable. When the eigenvalue is larger than 4, the associated eigenmode is unstable.
3) The equality of CFL condition corresponds to the situation where the largest eigenvalue is equal to 4. When the CFL condition is satisfied, the FDTD solutions contain only the stable modes and when the CFL condition is not satisfied, the FDTD solutions contain both the stable and unstable modes. If the unstable modes can be removed, the FDTD solutions can remain stable.
4) Even when the CFL condition is satisfied, the FDTD solutions may become unstable if the sources or excitations have the same poles as those of the eigenmodes. For a problem of a large physical domain that has a large number of electric field nodes, the size of **M** can be huge so is the number of the poles of the FDTD system. The poles may be cluster densely together and it is harder for the sources or excitations to avoid having the poles of the FDTD systems, instability may occur more frequently.

2.4 THE UNCONDITIONALLY STABLE WAVE-EQUATION BASED FDTD METHOD

As mentioned before, eigenvectors of **M** do not change with the time steps chosen but eigen values do. Given a time step, eigenvalues can be determined, and so can the stability of the corresponding eigenvectors. In other words, a stable FDTD solution can be obtained by removing the unstable eigenvectors in a FDTD solution. It will be elaborated below.

2.4.1 The Proposed Unconditionally Stable Method

The first step of the proposed method is to derive the eigenvalues and eigenvectors of the FDTD system matrix which is sparse. The stable eigenmodes are actually the eigenvectors of **M** that have the eigenvalues of smaller than 4. Direct solutions of eigenvalues and eigenvectors of **M** is not practical if the size of the FDTD system is large. There are various methods (e.g., power method, Lanczos Iteration, Arnoldi Iteration) and

software packages to find eigenvalues and eigenvectors (modes) of a matrix accurately and efficiently. Among them, the implicitly restarted Arnoldi algorithm [46] is very robust and efficient and it is adopted by sophisticated software like Matlab®.

Alternatively, a simple procedure, as presented in [26, 47], can be applied to find a limited number of physically important stable eigenvectors. The procedure starts from a trial conventional FDTD simulation of a limited number of marching iterations, say from n=1 to k. The time step is chosen to satisfy the CFL condition. At each time incidence, the FDTD solution is orthonormalized with previous solution vectors and stored in a matrix **S**. By applying the following order reduction process,

$$\mathrm{R}_{k*k} = \mathrm{S}^{T}{}_{k*Ne}\mathrm{M}_{Ne*Ne}\mathrm{S}_{Ne*k} \tag{2.28}$$

in which N_e is the number of unknown electric field nodes. Since k is chosen much smaller than N_e i.e. k<< N_e, R_{k*k} is a small matrix and a common eigen-solver could be applied to it and find the eigenvalues and eigenvectors at little cost. Denote the corresponding eigenvectors found as V_R. Then the physically important eigenvectors of **M**, denoted as **V**, can be found as:

$$\mathrm{V}_{Ne*1} = \mathrm{S}_{Ne*k}\mathrm{V}_{Rk*1} \tag{2.29}$$

The procedure is terminated when the new solution vector has negligible component orthogonal with the space defined by **V**:

$$\frac{\left\| E(n) - VV^{T}E(n) \right\|}{\left\| E(n) \right\|} \le 10^{-3} \tag{2.30}$$

10^{-3} is a prescribed error that can also be other small values.

Suppose that a time step is chosen, for instance, p times of the CFL limit. Then the stable modes (denoted as $\mathbf{V}_s$) can be selected from the eigenvectors and expressed as:

$$\{V_s\} = \left\{ V_{\lambda<4/p^2} \right\} \tag{2.31}$$

In other words, the unstable eigenvectors are discarded. The FDTD solution of electric fields can then be projected on the sub-space $\{V_s\}$ composed of these stable modes expressed in the equation below:

$$\mathrm{E} = V_s V_s^{'} \mathrm{E} \tag{2.32}$$

Another thing which should be paid attention is not all eigenmodes have the same weights or are physically important in the solution. Some eigenmodes may have negligible even zero weight in the solution. The weights of the eigenmodes or eigenvectors in the solution are determined by the sources or excitations in a linear medium; they can be obtained with the inner products of the eigenvectors with the sources or eigenvectors.

Another way to find the weights of the eigenmodes is to run a short run of the FDTD solution and the weights of the eigenmodes can be derived by inner product of the FDTD solution obtained and the eigenmodes. The modes that have negligible weights can be ignored. By doing this, the number of stable modes in the FDTD solutions can be further reduced and the computation will become more efficient.

Based on the above analysis, we propose the stable FDTD solution as follows:

[1] Given a time step, apply the procedure (2.28) to (2.31) and find the stable and physically important modes of **M**, $\{V_s\}$.

[2] Run initial two steps of the FDTD simulation with a time step which could be larger than the CFL limit.

[3] Expand the FDTD solutions in terms of (2.5) to project the FDTD solution of electric fields to the sub-space defined by $\{V_s\}$. Derive the expansion coefficient $a_i[0]$ and a_i [1] for each stable eigenmode.

[4] Use (2.9) to find all the coefficients a_i [n] and (2.5) to obtain electric fields.

[5] Find magnetic fields from the obtained electric fields through Maxwell's equations.

2.4.2 Numerical Experiments

In the following paragraphs, the proposed method is tested with a practical case. An "H" shape cavity is considered, as shown in Figure 2.8. TM waves inside the cavity are simulated and observed. Due to the narrow gap in the cavity, fine grids are employed to obtain good modeling accuracy. As a result, with the FDTD method, the upper limit of the time step, as restricted by the small space grid size, is small; the simulation will take a relatively long time and relatively large memory.

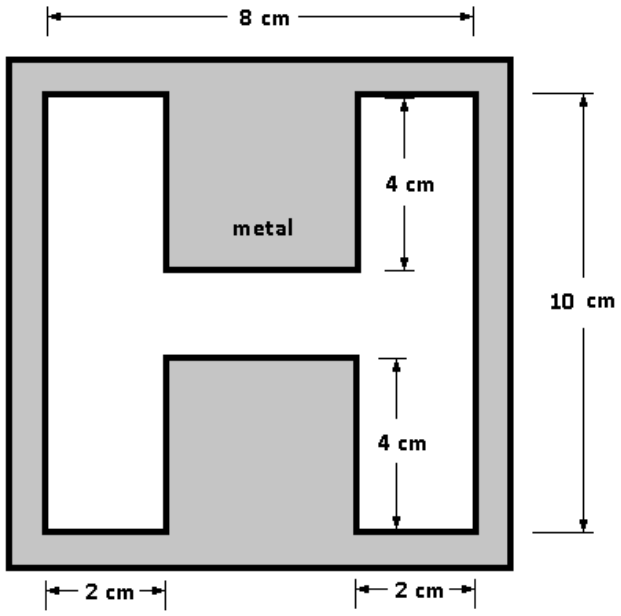

Figure 2.8 Structure of the H type metal cavity.

With the proposed method, we can choose a large time step, apply the solution steps described above, and obtain a stable solution. A uniform numerical grid is used with a cell size of $1mm \times 1mm$. A Gaussian pulse is excited at the center of the cavity.

Figure 2.9 and Figure 2.10 show the numerical results. By taking the discrete Fourier transform of the solutions, the frequency domain solutions are obtained and shown in Figure 2.9. As can be seen, the results of the proposed method agree well with those of the conventional FDTD method except high-frequency components; this is expected since the high frequency components correspond to unstable modes and are discarded with the proposed method.

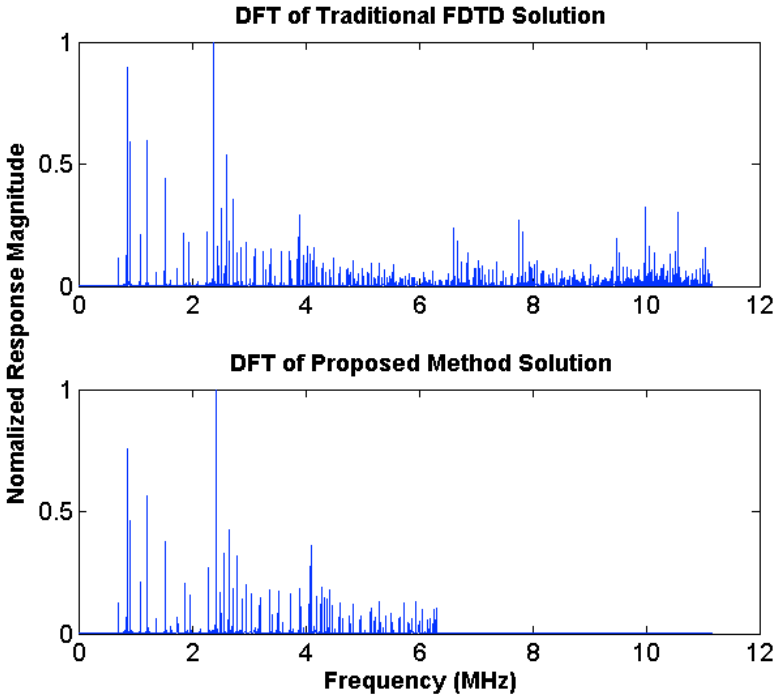

Figure 2.9 Frequency responses obtained with the conventional FDTD and the proposed method.

Figure 2.10 shows the field distributions obtained with the conventional FDTD method and the proposed method. The first one of Figure 2.10 is the normalized field distribution at the 100,000th time step, obtained with the conventional march-on-time recursive FDTD simulation. The time step is 11.18ns which is 0.5 of the CFL limit. The second one is the field distribution at the 25,000th time step, obtained with the proposed method. The time step was 44.72ns which is two times of the CFL limit and four times of the time step used with the conventional FDTD simulation. In other words, 25,000 time steps of the proposed FDTD method represent the same physical time of 100,000 time steps of the conventional FDTD simulation. The distributions are basically the same except that the high-order modes associated with the high frequencies are discarded with the proposed method.

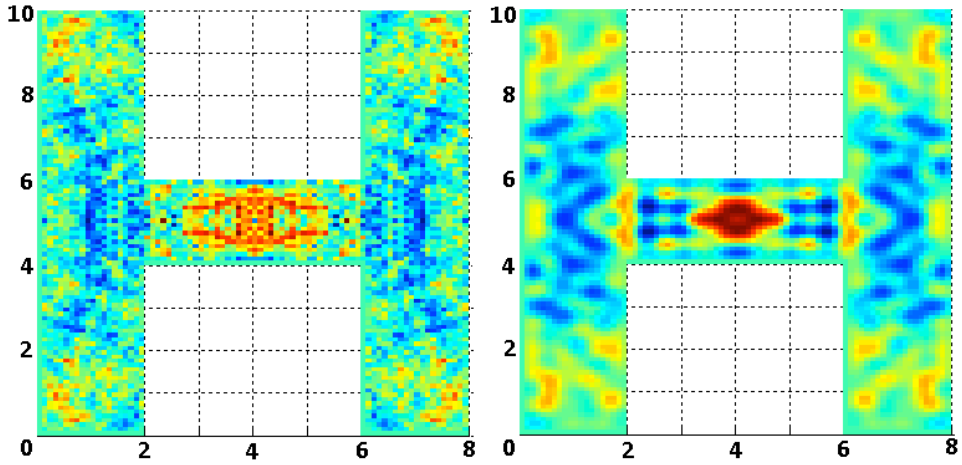

Figure 2.10 Electric field distribution obtained with the conventional FDTD simulation (left) and proposed method (right).

2.5 SUMMARY

In this chapter, based on the eigen analysis of the FDTD method, the root cause of the instability is revealed and explained using the concept of discrete systems and Z-transformation. The relationship between the CFL condition and the stability is revealed. An interesting phenomenon is found that the CFL condition does not always guarantee the stability of the FDTD solutions, if specific monochromatic source is injected into the system. Numerical examples verified the findings. Based on the above analysis, we propose an unconditionally stable wave-equation based FDTD method; in it, electric and magnetic fields are solved in a decoupled and simplified manner. Numerical FDTD solutions can then be expanded by a limited number of stable eigenmodes. Each eigenmode and corresponding eigenvalue can be calculated at $O(Ne^2)$ complexity. Once the eigenmodes are found, the solution can be simply obtained with the difference equations of coefficients instead of time-marching iterations. Numerical examples are presented to verify the effectiveness of the proposed method. Because of that the principles and developments are without much of theoretical restrictions, discussions and formulations presented in this chapter can be generalized and extended to other time domain numerical methods.

CHAPTER 3 ANALYTIC SOLUTION OF THE FDTD METHOD

3.1 INTRODUCTION

In Chapter 2, we have analyzed the FDTD method and proposed an alternative new FDTD solution process. More specifically, we have systematically investigated the FDTD formulation and developed the wave-equation based discrete system. We have transformed the system into a series of discrete scalar sub-systems and apply the Z-domain solutions for stability analyses. The final FDTD solutions are then obtained by solving the difference equations of the expansion coefficients.

In this chapter, as a further development and significant extension of the analysis of the previous chapter, we derive the analytic solutions of the FDTD method that do not require the conventional iterative march-on-in-time solution process. The FDTD solution can then be directly obtained at any given time desired. Other details pertinent to the analytic solutions, including source implementations, treatment of lossy media, are also presented. Finally, we numerically verify the proposed method and conclude that the analytic approach can serve as an alternative way to the solutions of the conventional FDTD method.

3.2 ANALYTIC FORM OF THE FDTD SOLUTION

In previous chapter, we have presented the wave-equation based FDTD method in its matrix form, which is

$$\mathbf{E}[n+1] + \mathbf{E}[n-1] - 2\mathbf{E}[n] + \mathbf{M}\mathbf{E}[n] = \mathbf{x}[n] \quad \text{(input)} \tag{3.1}$$

where matrix **M** is the FDTD system matrix as defined before.

Eigen-analysis is performed on (3.1). By expanding the electric field solution vector E[n] and the input term x[n] on the eigenvectors of matrix **M**,

$$\begin{aligned} &\mathbf{E}[n] = \mathbf{V}a[n] \\ &\mathbf{x}[n] = \mathbf{V}b[n] \quad \text{or} \quad b[n] = \mathbf{V}^{-1}\mathbf{x}[n] = \mathbf{V}'\mathbf{x}[n] \end{aligned} \tag{3.2}$$

As derived in the previous chapter, (3.1) can finally turn into the difference equation of coefficient a_i for each eigenvector, as expressed by (2.9):

$$a_{i,n+1} + a_{i,n-1} - (2 - \lambda_i) a_{i,n} = b_{i,n}, \text{ for } n = 1, 2, 3, \ldots \tag{3.3}$$

(3.3) is the difference equation for coefficient a_i which can be solved iteratively. It can also be considered as a discrete system, whose response can be derived using the Z-transform:

$$\begin{aligned} & zA_i[z] + z^{-1}A_i[z] - 2A_i[z] + \lambda_i A_i[z] = B_i[z] \ , \\ & H_i[z] = \frac{A_i[z]}{B_i[z]} = \frac{z}{z^2 + 1 - (2 - \lambda_i)z}. \end{aligned} \tag{3.4}$$

The impulse response in the time domain is

$$h_i[n] = \frac{1}{(z_{i,1} - z_{i,2})}(z_{i,1})^{n-1} + \frac{1}{(z_{i,2} - z_{i,1})}(z_{i,2})^{n-1} \tag{3.5}$$

As discussed, when the CFL condition is met, the eigenvalues of matrix **M** is within the range (0,4), which ensures the system poles on the unit circle in the Z-domain. The two poles, z_{i1} and z_{i2}, are conjugate to each other and are on the unit circle, which can be expressed as

$$z_{i1,2} = e^{j\theta_{i1,2}} = \frac{(2 - \lambda_i) \pm j\sqrt{4\lambda_i - \lambda_i^{\,2}}}{2} \quad . \tag{3.6}$$

The angles are

$$\begin{aligned} & \theta_{i1} = \arctan\left(\frac{\sqrt{4\lambda_i - \lambda_i^{\,2}}}{2 - \lambda_i} \right) \ , \\ & \theta_{i2} = -\theta_{i1} \quad . \end{aligned} \tag{3.7}$$

Correspondingly, the impulse response (3.5) for this stable system can be expressed as

$$
\begin{aligned}
h_i[n] &= \frac{1}{(z_{i,1}-z_{i,2})}(z_{i,1})^{n-1} + \frac{1}{(z_{i,2}-z_{i,1})}(z_{i,2})^{n-1} \\
&= \frac{1}{2i\sin\theta_i}[\cos(n-1)\theta_i + i\sin(n-1)\theta_i] \\
&\quad + \frac{1}{-2i\sin\theta_i}[\cos(n-1)\theta_i - i\sin(n-1)\theta_i] \\
&= \frac{\sin[(n-1)\theta_i]}{\sin\theta_i} \qquad \text{with} \quad h_i[0] = h_i[1] = 0
\end{aligned}
\tag{3.8}
$$

Equation (3.8) is the stable impulse solution of the FDTD system as described by (3.1).

Consider now Kronecker impulse excitation that has non-zero value at time incidence n=1, i.e., $b[1] = [b_{1,1}\ b_{2,1}\ \ldots\ b_{i,1}\ \ldots\ b_{N_e,1}]^T$ is not zero and the excitation at other time instances $b[n]_{\ n=2,3,\ldots}$ is zero. In other words, at initial time n=1, every eigen mode V_i is excited with an amplitude of $b_{i,1}$. Then

$$
B_i(z) = b_{i,1} \quad , \tag{3.9}
$$

and the initial amplitude of $\mathbf{V}_i$ is

$$
\begin{aligned}
a_{i,n} &= Z^{-1}\{B_i(z)H_i(z)\} = Z^{-1}\{b_{i,1}H_i(z)\} \\
&= b_{i,1}h_i(n) = b_{i,1}\frac{\sin[(n-1)\theta_i]}{\theta_i}
\end{aligned}
\tag{3.10}
$$

As a result, by (3.3), the FDTD solution is:

$$
\begin{aligned}
\mathrm{E}[n] = \mathrm{V}a[n] &= \mathrm{V}\begin{bmatrix} a_{1,n} \\ \ldots \\ a_{i,n} \\ \ldots \\ a_{i,N_e} \end{bmatrix} = [\mathrm{V}_1 a_{1,n} \quad \ldots \quad \mathrm{V}_i a_{i,n} \quad \ldots \quad \mathrm{V}_{N_e} a_{N_e,n}] \\
&= [\mathrm{V}_1 b_{1,1}h_1(n) \quad \ldots \quad \mathrm{V}_i b_{i,1}h_i(n) \quad \ldots \quad \mathrm{V}_{N_e} b_{1,1}h_{N_e}(n)] \\
&= [\mathrm{V}_1 b_{1,1}\frac{\sin[(n-1)\theta_1]}{\sin\theta_1} \quad \ldots \quad \mathrm{V}_i b_{i,1}\frac{\sin[(n-1)\theta_i]}{\sin\theta_i} \quad \ldots \quad \mathrm{V}_{N_e} b_{1,1}\frac{\sin[(n-1)\theta_{N_e}]}{\sin\theta_{N_e}}]
\end{aligned}
\tag{3.11}
$$

In most practical cases, the source signal has a duration. Consider that the source has a duration of sequential M impulses. In such a case, because the FDTD system is a linear system, the field solution as a result of excitation $b_{i,k}$ at the k-th time step can be considered the same as that due to $b_{i,1}$ in (3.11), except delayed by k time steps and a change of amplitude from $b_{i,0}$ to $b_{i,k}$. The overall FDTD solutions will be the sum of the responses due to all the source amplitudes of from $b_{i,0}$ to $b_{i,k}$. In other words, the full FDTD solutions are then:

$$\mathrm{E}[n] = \mathrm{V}\begin{bmatrix} \sum_{k=1}^{M} b_{1,k} h_1(n-k)u(n-k) \\ \cdots \\ \sum_{k=1}^{M} b_{i,k} h_i(n-k)u(n-k) \\ \cdots \\ \sum_{k=1}^{M} b_{N_e,k} h_{N_e}(n-k)u(n-k) \end{bmatrix} = \mathrm{V}\begin{bmatrix} \sum_{k=1}^{M} b_{1,k} \dfrac{\sin(n-k)\theta_1}{\sin\theta_1} u(n-k) \\ \cdots \\ \sum_{k=1}^{M} b_{i,k} \dfrac{\sin(n-k)\theta_i}{\sin\theta_i} u(n-k) \\ \cdots \\ \sum_{k=1}^{M} b_{N_e,k} \dfrac{\sin(n-k)\theta_{N_e}}{\sin\theta_1} u(n-k) \end{bmatrix} \quad (3.12)$$

In the above equation, function $u(n)$ is the unit function that is unitary at $n \geq 0$ and zero otherwise.

Equation (3.12) is the explicit analytical expression of the FDTD solution. The FDTD solution is a function of discrete time step n and can be obtained directly at any time instant n as long as the eigenvalues and vectors of **M** are known or found in advance.

3.3 THE HARD SOURCE IMPLEMENTATION

Analysis above is based on the soft source settings. A soft source means that the source is simply added to the current field value at the source nodes, which can be considered as a simple input of the system. For the cases with the hard sources, on the other hand, the source nodes are assigned with certain field values, or boundary nodes are imposed with fixed boundary conditions; the source field values are not additive to the current field values but imposed on them.

Consider the conventional FDTD leap-frog scheme

$$\begin{aligned} \mathrm{H}[n+\frac{1}{2}] &= \mathrm{H}[n-\frac{1}{2}] - \Delta t \mathrm{D}_E \mathrm{E}[n] \\ \mathrm{E}[n+1] &= \mathrm{E}[n] + \Delta t \mathrm{D}_H \mathrm{H}[n+\frac{1}{2}] \end{aligned} \tag{3.13}$$

in which matrixes D_E and D_H follows the same definition as those of (2.2).

Now decompose the electric field vector $\mathrm{E}[n]$ of the whole problem region into two sets: the field value on the hard source (or forced boundary) nodes $\mathrm{E}_s[n]$, and those on other electric nodes $\mathrm{E}_u[n]$ whose value are unknown and need to be solved. The decomposition can be written as

$$\mathrm{E}[n] = \begin{bmatrix} \mathrm{E}_u[n] \\ \mathrm{E}_s[n] \end{bmatrix} \tag{3.14}$$

Denote the number of unknown electric field nodes as $N_{e,u}$, the number of source and known-boundary nodes as $N_{e,s}$, and N_h as the number of magnetic field nodes. Correspondingly, matrix D_E and D_H can be rewritten into two blocks with respect to the decomposition of electric field vector $\mathrm{E}[n]$. The matrix D_E can be partitioned as

$$\mathrm{D}_E = [\mathrm{D}_{E,u} \;\; \mathrm{D}_{E,s}] \tag{3.15}$$

in which $\mathrm{D}_{E,u}$ is the matrix of $N_h \times N_{e,u}$, represents $\mu^{-1}\nabla\times$ operation on the unknown electric nodes for updating the magnetic field. $\mathrm{D}_{E,s}$ is the matrix of $N_h \times N_{e,s}$, representing the same operation on electric field nodes (and forced boundary nodes.) Similarly, the matrix D_H can be decomposed as

$$\mathrm{D}_H = \begin{bmatrix} \mathrm{D}_{H,u} \\ \mathrm{D}_{H,s} \end{bmatrix}. \tag{3.16}$$

in which $\mathrm{D}_{H,u}$ is the matrix of size $N_{e,u} \times N_h$, represents the discretized $\varepsilon^{-1}\nabla\times$ operator at the position of unknown magnetic nodes for updating the electric field.

$\mathrm{D}_{H,s}$ is of size $N_{e,s} \times N_h$, representing the same operator for updating the electric hard source and forced boundary nodes.

Based on these notations, the update equations (3.13) can be rewritten as

$$\begin{aligned} \mathrm{H}[n+\frac{1}{2}] &= \mathrm{H}[n-\frac{1}{2}] - \Delta t \begin{bmatrix} \mathrm{D}_{E,u} & \mathrm{D}_{E,s} \end{bmatrix} \begin{bmatrix} \mathrm{E}_u[n] \\ \mathrm{E}_s[n] \end{bmatrix} \\ \begin{bmatrix} \mathrm{E}_u[n+1] \\ \mathrm{E}_s[n+1] \end{bmatrix} &= \begin{bmatrix} \mathrm{E}_u[n] \\ \mathrm{E}_s[n] \end{bmatrix} + \Delta t \begin{bmatrix} \mathrm{D}_{H,u} \\ \mathrm{D}_{H,s} \end{bmatrix} \mathrm{H}[n+\frac{1}{2}] \end{aligned} \tag{3.17}$$

Since the field values at the hard source nodes or forced boundaries are known or specified, update of E_s are not needed and (3.17) can be simplified as:

$$\begin{aligned} \mathrm{H}[n+\frac{1}{2}] &= \mathrm{H}[n-\frac{1}{2}] - \Delta t \mathrm{D}_{E,u} \mathrm{E}_u[n] - \Delta t \mathrm{D}_{E,s} \mathrm{E}_s[n] \\ \mathrm{E}_u[n+1] &= \mathrm{E}_u[n] + \Delta t \mathrm{D}_{H,u} \mathrm{H}[n+\frac{1}{2}] \end{aligned} \tag{3.18}$$

The update of electric field is now performed on E_u only. (3.18) can be further reduced to the wave equation by substituting the expression for H into the expression for E_u:

$$\mathrm{E}_u[n+1] + \mathrm{E}_u[n-1] - 2\mathrm{E}_u[n] + \Delta t^2 \mathrm{D}_{H,u} \mathrm{D}_{E,u} \mathrm{E}_u[n] = -\Delta t^2 \mathrm{D}_{H,s} \mathrm{D}_{E,s} \mathrm{E}_s[n] \tag{3.19}$$

Apparently, the above wave equation has the form similar to the FDTD equations of (3.1) for the soft sources. The differences are that (3.19) updates unknown electric field E_u only and the hard source fields (including the forced boundary conditions) E_s is transformed into an equivalent soft source term $-\Delta t^2 \mathrm{D}_{H,s} \mathrm{D}_{E,s} \mathrm{E}_s[n]$ on the right hand side of the equation. The resulting equation fits well with the form of (3.1). By eigen-analysis of the new system matrix $\Delta t^2 \mathrm{D}_{H,u} \mathrm{D}_{E,u}$ of (3.19), the explicit analytic solution can be derived with the similar format of equation (3.12).

3.4 THE EXPLICIT ANALYTICAL FDTD SOLUTION IN A LOSSY MEDIUM

In the cases of lossy medium, Maxwell equations become

$$\nabla \times \mathbf{E} = -\mu \frac{\partial \mathbf{H}}{\partial t}$$
$$\nabla \times \mathbf{H} = \sigma \mathbf{E} + \varepsilon \frac{\partial \mathbf{E}}{\partial t} + \mathbf{J} \quad , \tag{3.20}$$

where σ is the conductivity of the medium.

By following the same FDTD discretization process of (2.1)-(2.4) (as applied in the above sections in this chapter), the recursive discrete electric wave equation in the lossy medium can be obtained as

$$\left(1+\frac{\sigma\Delta t}{2\varepsilon}\right)\mathbf{E}[n+1]+\left(1-\frac{\sigma\Delta t}{2\varepsilon}\right)\mathbf{E}[n-1]-(2-\mathbf{M})\mathbf{E}[n]=\mathbf{x}[n] \tag{3.21}$$

The quantities are defined in the same way as those defined at (2.4) in the lossless case.

Again, by expanding $\mathbf{E}[n]$ and $\mathrm{x}[n]$ in terms of the eigenvectors of **M**, (3.21) becomes a series of recursive equations:

$$\left(1+\frac{\sigma\Delta t}{2\varepsilon}\right)a_i[n+1]+\left(1-\frac{\sigma\Delta t}{2\varepsilon}\right)a_i[n-1]-(2-\lambda_i)a_i[n]=b_i[n] \tag{3.22}$$
$$\text{for } i=1,2,3...$$

Application of the unilateral *Z*-transform to the above equation leads to

$$\left(1+\frac{\sigma\Delta t}{2\varepsilon}\right)zY_i[z]+\left(1-\frac{\sigma\Delta t}{2\varepsilon}\right)z^{-1}Y_i[z]-2Y_i[z]+\lambda_i Y_i[z]=X[z] \tag{3.23}$$

$$H_i[z]=\frac{Y_i[z]}{X[z]}=\frac{1}{\left(1+\frac{\sigma\Delta t}{2\varepsilon}\right)}\frac{z}{z^2-\frac{(2-\lambda_i)}{\left(1+\frac{\sigma\Delta t}{2\varepsilon}\right)}z+\frac{\left(1-\frac{\sigma\Delta t}{2\varepsilon}\right)}{\left(1+\frac{\sigma\Delta t}{2\varepsilon}\right)}} \tag{3.24}$$

Stability of this system depends on the poles of the transfer function above. Detailed analysis (see Appendix II) will show that in lossy cases, $0<\lambda_i<4$ for all the eigenvalues is still the necessary condition for stable FDTD solutions, whereas $\lambda_i > 4$ will lead to unstable FDTD solutions.

Now assume that $0<\lambda_i<4$. Analytical solutions to the recursive equations of (3.23) can be obtained. There are two cases to consider:

Case 1: $0<\lambda_i<4$ and $\lambda_i^2-4\lambda_i+\frac{\sigma^2\Delta t^2}{\varepsilon^2}>0$

The two poles are real numbers that can be expressed as:

$$z_{i,1or2}=\frac{2-\lambda_i\pm\sqrt{\lambda_i^2-4\lambda_i+\frac{\sigma^2\Delta t^2}{\varepsilon^2}}}{2+\frac{\sigma\Delta t}{\varepsilon}} \tag{3.25}$$

the impulse response of this system is

$$\begin{aligned} h_i[n] &= \frac{1}{\left(1+\frac{\sigma\Delta t}{2\varepsilon}\right)}\frac{1}{z_{i,1}-z_{i,2}}\left(z_{i,1}^{\,n-1}-z_{i,2}^{\,n-1}\right) \\ &= \frac{1}{\left(1+\frac{\sigma\Delta t}{2\varepsilon}\right)}\frac{2+\frac{\sigma\Delta t}{\varepsilon}}{2\sqrt{\lambda_i^2-4\lambda_i+\frac{\sigma^2\Delta t^2}{\varepsilon^2}}}\left(z_{i,1}^{\,n-1}-z_{i,2}^{\,n-1}\right) \quad . \\ &= \frac{z_{i,1}^{\,n}-z_{i,2}^{\,n}}{\sqrt{\lambda_i^2-4\lambda_i+\frac{\sigma^2\Delta t^2}{\varepsilon^2}}} \end{aligned} \tag{3.26}$$

The above solution can be verified by substituting it into (3.22) with the initial conditions of $h_i[0]=h_i[1]=0$. Since magnitudes of $z_{i,1}$ and $z_{i,2}$ are smaller than 1 (see Appendix II), $h_i[n]$ will be damped to zero as time progresses.

Case 2: $0<\lambda_i<4$ and $\lambda_i^2-4\lambda_i+\frac{\sigma^2\Delta t^2}{\varepsilon^2}<0$.

The two poles are conjugate complex numbers that can be expressed as

$$z_{i,1or2}=\frac{2-\lambda_i\pm j\sqrt{4\lambda_i-\lambda_i^2-\frac{\sigma^2\Delta t^2}{\varepsilon^2}}}{2+\frac{\sigma\Delta t}{\varepsilon}} \quad . \tag{3.28}$$

Their angles and magnitudes are

$$\theta_{i1} = \arctan\left(\frac{\sqrt{4\lambda_i - \lambda_i^{\,2} - \dfrac{\sigma^2\Delta t^2}{\varepsilon^2}}}{2-\lambda_i}\right)$$

$$\theta_{i2} = -\theta_{i1} \qquad . \qquad (3.29)$$

$$\left|z_{i,1}\right| = \left|z_{i,2}\right| = z_i = \frac{\sqrt{4 - \dfrac{\sigma^2\Delta t^2}{\varepsilon^2}}}{2 + \dfrac{\sigma\Delta t}{\varepsilon}} < 1$$

The impulse response of this system is

$$\begin{aligned} h_i[n] &= \frac{1}{\left(1+\dfrac{\sigma\Delta t}{2\varepsilon}\right)} \frac{1}{z_{i,1} - z_{i,2}} (z_1^{\,n-1} - z_2^{\,n-1}) \\ &= \frac{1}{\left(1+\dfrac{\sigma\Delta t}{2\varepsilon}\right)} \frac{1}{z_i (e^{j\theta_i} - e^{-j\theta_i})} z_i^{\,n} (e^{j(n-1)\theta_i} - e^{-j(n-1)n\theta_i}) \qquad . \qquad (3.30) \\ &= \frac{1}{\left(1+\dfrac{\sigma\Delta t}{2\varepsilon}\right)} z_i^{\,n-1} \frac{\sin[(n-1)\theta_i]}{\sin\theta_i} \end{aligned}$$

Since $z_{i,1}$ and $z_{i,2}$ are conjugate complex numbers with magnitude smaller than 1, the FDTD impulse response will be oscillating and decaying to zero as time progresses (i.e., n increases).

Once $h_i[n]_{\,i=1,2,\ldots,N_e}$ are obtained, the FDTD solution can be found through similar procedure as that for the lossless case (3.10~3.12).

3.5 Summary Of Analytic Solution Of The FDTD Method

From the analysis and results presented in chapter two, solutions of the FDTD method can be expanded in terms of fixed eigenmodes with time-dependent expansion

coefficients. Instead of solving the time-dependent coefficient numerically, the explicit analytical expressions of the coefficients can be obtained by solving the discrete system using the Z-transformation and so can the FDTD solutions at any time incidence. More specifically, the steps to obtain the FDTD solutions can be summarized below:

1) Choose time step Δt, construct the discrete system in the wave equation form of (3.1) and obtain matrix **M** (which is the discretized finite-difference form of operator $\Delta t^2(\varepsilon\mu_0)^{-1}\nabla\times\nabla\times$). We could choose the time step which satisfies the CFL condition to obtain the analytic solution formulation. The choice does not affect the efficiency of the method, since the solution at any time incidence will be solved analytically without iterative process.
2) Apply known efficient algorithms or software packages (e.g., [16]) to find physically important eigenvectors (or eigenmodes) with the corresponding eigen values $0<\lambda_i<4$.
3) For any given time incidence *n*, compute (3.12) to find mode amplitude $b[n]$ for each mode.
4) Use (3.2) to obtain electric fields $\mathbf{E}[n]$.
5) Find magnetic fields from the obtained electric fields through Maxwell's equations (2.1).

Compared with the conventional FDTD solution approach, the above proposed method involves eigen-decomposition to system matrix **M** which is a sparse and symmetric matrix. Therefore, the computational efficiency of the proposed method is very much dependent on the algorithms used to extract the eigenvalues and eigenvectors. Various mathematical algorithms have been developed for efficient eigen-decomposition of a real, sparse, semi positive-definitive and symmetric matrix. After eigen-decomposition is done, analytical FDTD solutions are obtained at almost no additional computational costs. Comparisons between the proposed FDTD solution approach and the conventional FDTD iterative method are not easy to make due to the different solutions paths. However, two obvious advantages of the proposed method over the conventional approach can be seen in either one of the two situations: 1) when an FDTD

solution requires a long iteration such that the iteration time exceeds the time in extracting the eigenvalues and eigenvectors of the stable modes, and 2) when the FDTD solutions of a structure need to be stored or recorded. In addition, since only electric or magnetic field is dealt with, the proposed approach uses less memory than the conventional FDTD solution approach where both electric and magnetic fields are simultaneously solved.

Although the above analyses are performed on the FDTD method, they can be extended to other march-on-time numerical methods since recent studies have indicated that numerical methods are of the same nature in their solutions and can be unified with the same numerical mathematical framework [48, 49].

In the next section, numerical experiments are carried out using the proposed method.

3.6 NUMERICAL EXPERIMENTS

To verify the proposed analytical FDTD solution presented above, two structures were computed as examples. The first is an "H" shape cavity as shown in Fig. 3.1 and the second one is the dielectric rod which is shown later. The cavity is chosen because it is not only a simple structure with readily available analytical solutions for comparisons but also embodies multiple field scatterings and reflections of electromagnetic waves from the cavity walls. If a method or an approach is incorrectly formulated, such multiple waves will be wrongly simulated, appear in the results, and can be easily identified. In other words, cavities present solid and convincing tests of a numerical method. The experiments are elaborated and described as follows.

3.6.1 Numerical Experiment I: Analytic FDTD solution of the H-shape Cavity

The first experiment is performed on an H-shape cavity. It is shown in Figure 3.1. A uniform numerical cell size of 1 mm $\times$1 mm $\times$1 mm was used to discretize the cavity. A Gaussian pulse was excited at the center of the cavity. TM waves are simulated and observed for 2×10^5 steps. The time step size was chosen equal to the CFL limit. For

comparisons, both the proposed and conventional FDTD solution approaches were carried out.

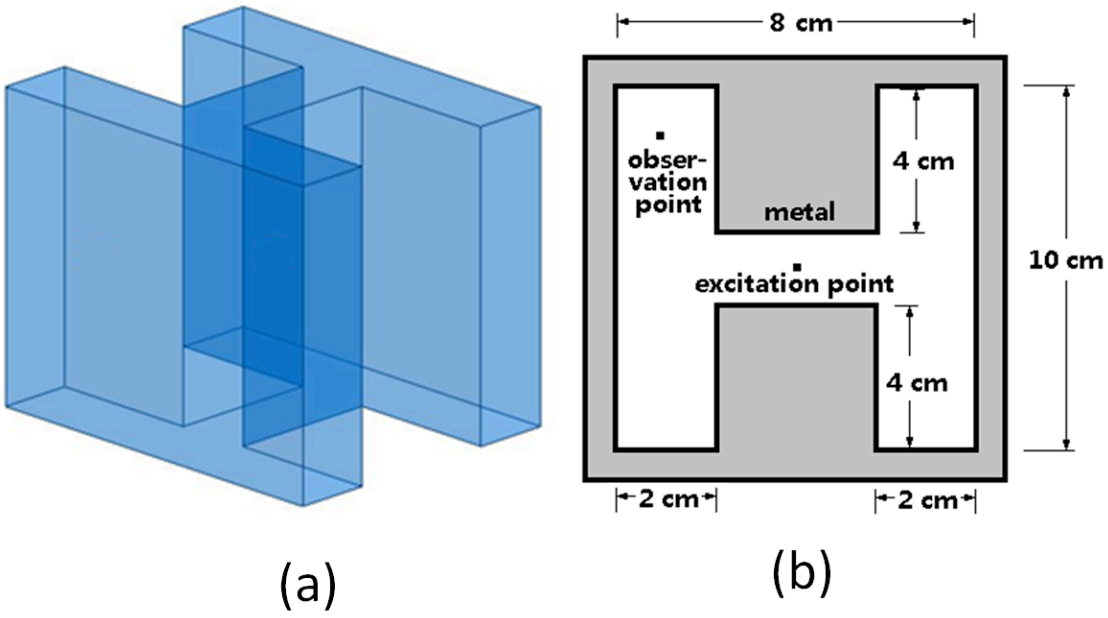

Figure 3.1 Structure of H type metal cavity: (a) the three-dimensional view, (b) the cross-sectional view.

Figure 3.2 and Figure 3.3 show the field distributions obtained with the two methods. The differences between the results are normalized to the largest values of the transient fields. As can be seen, the field distributions are visibly the same and the relative differences between the results obtained with the two methods are extremely small, namely at the noise level.

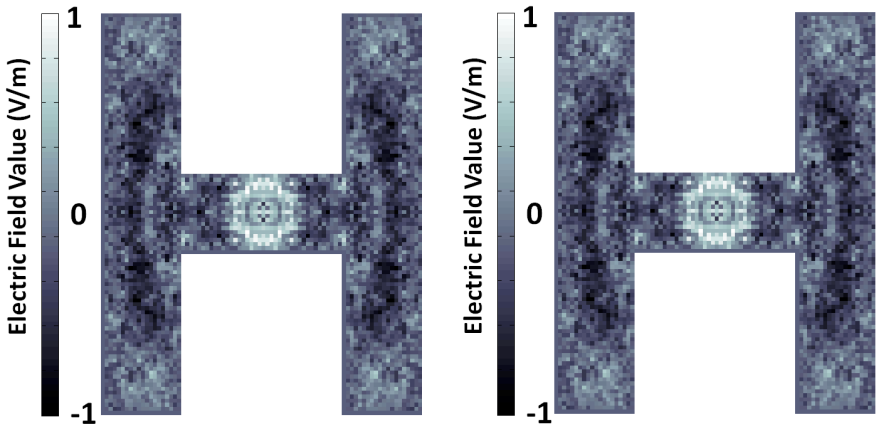

Figure 3.2 Field distribution recorded at the 200,000th time step of proposed method (left) and the conventional FDTD method (right).

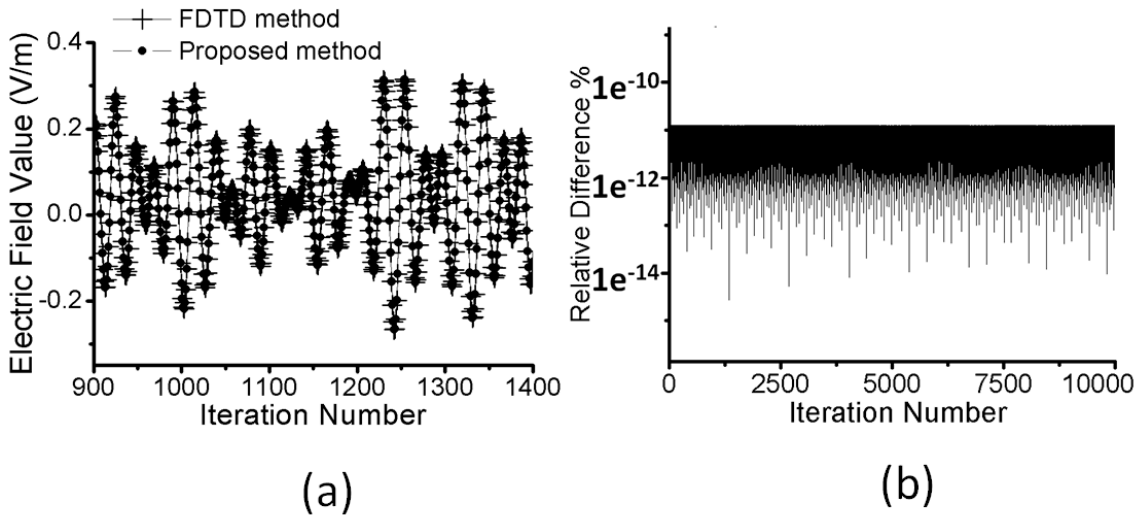

Figure 3.3 Results (recorded at the observation point) obtained with the proposed and the conventional FDTD methods. (a) shows the field values obtained by the two methods at observation node and (b) shows their relative errors for a 10^4 steps simulation. The errors are below 10^{-11}.

3.6.2 Numerical Experiment II: Simulation with Hard Source in Lossy Medium

The second experiment is to test the proposed scheme for hard source and in lossy medium settings. The simulation is performed with the conventional FDTD scheme and the proposed method for comparisons. In this experiment, the same cavity structure as that of Figure 3.1 is simulated but instead of air, lossy medium of conductivity σ of 0.1 S/m is filled in the cavity. The source is placed at the center of the cavity and is set to be a hard source, which forces the electric field to be 1V/m at the source. The time step size was chosen equal to the CFL limit. The electric field at the observation point is recorded for each time incidence *n*. Comparison of the results is shown in below:

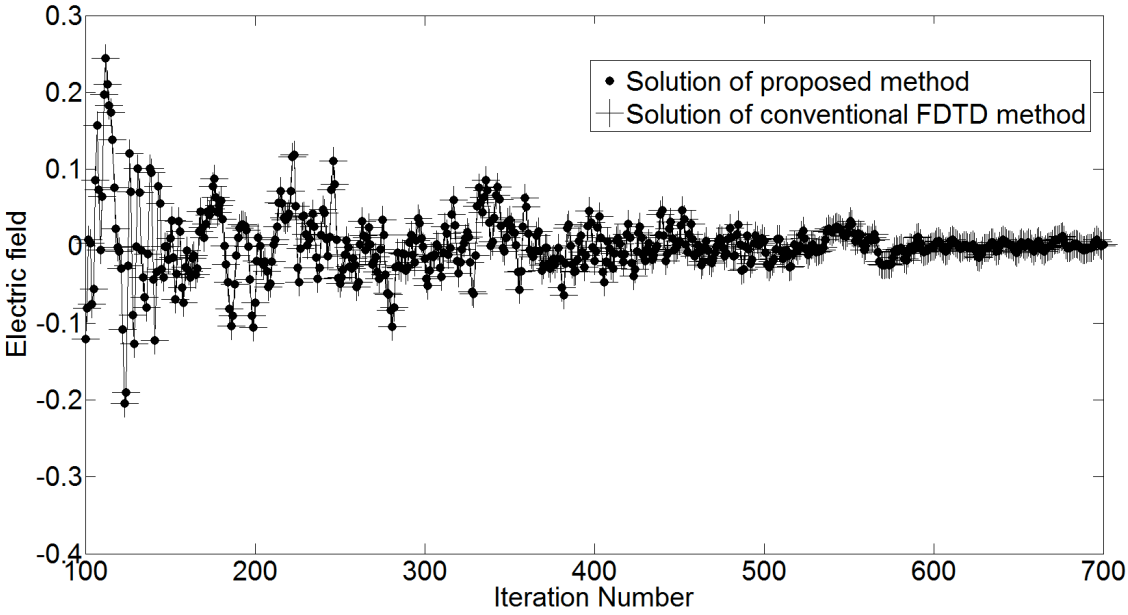

Figure 3.4 Results (recorded at the observation point) of field values obtained with the proposed and the conventional FDTD methods for the lossy-medium and hard source case.

As shown in Figure 3.4, it can be seen that the two solutions agree well with each other. The differences are below 10^{-11}, showing that the derived analytical FDTD solutions for lossy-medium and hard source are correct.

3.6.3 Numerical Experiment III: Simulation of the Dielectric Rod Structure

In the third numerical experiment, a dielectric rod resonator in a metallic rectangular cavity is considered as shown in Figure 3.5. The parameters of the dielectric resonator are chosen in accordance with the model used in [50, 51] : $2a$=2.5362 cm, b=2.5362 cm, h=0.6985 cm and l=2.5718 cm. The support of the dielectric rod is assumed to have dielectric constant of 1. The rod has a dielectric constant of 38. In the experiments, the size of the structure $2a \times b \times l$ is discretized into a numerical grid of $26 \times 26 \times 26$ and $31 \times 31 \times 32$, respectively.

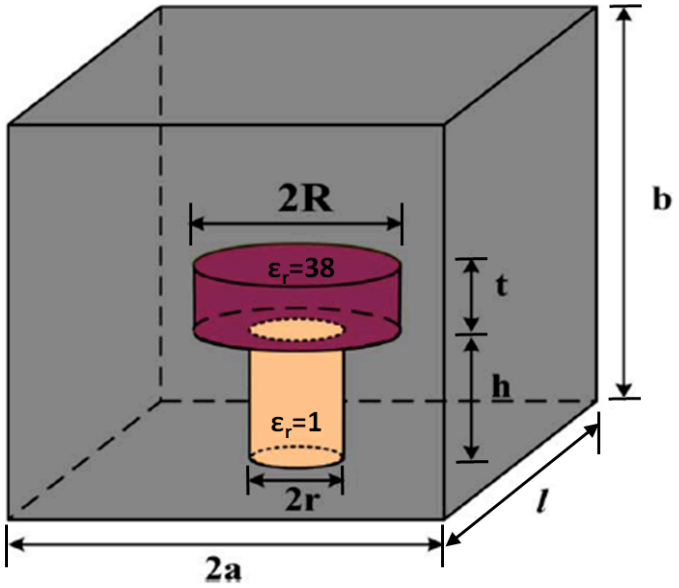

Figure 3.5 Geometry of the dielectric rod resonator in rectangular cavity.

The electric field wave equation for this dielectric-loaded structure can be found as:

$$\mathbf{E}[n+1]+\mathbf{E}[n-1]-2\mathbf{E}[n]+[\varepsilon_r]^{-1}\mathbf{M}\mathbf{E}[n]=\mathbf{x}[n] \quad \text{(input)} \tag{3.32}$$

in which $[\varepsilon_r]$ is the diagonal matrix of dielectric constant. The dielectric constant is a value which is a real number and larger than 1.

Compared with (3.1), apparently, $[\varepsilon_r]^{-1}\mathbf{M}$ is not necessarily semi-positive definite because it is not necessarily a symmetric matrix. Therefore, the method proposed in the previous discussion cannot be applied directly. To address this, (3.32) is reformulated and a variation of Maxwell wave equation for non-uniform dielectric medium cases is developed:

$$\begin{aligned}
&\overline{\mathbf{E}}[n+1]+\overline{\mathbf{E}}[n-1]-2\overline{\mathbf{E}}[n]+\overline{\mathbf{M}}\,\overline{\mathbf{E}}[n]=\overline{\mathbf{x}}[n]\\
&\overline{\mathbf{E}}=[\varepsilon_r]^{1/2}\mathbf{E},\quad \overline{\mathbf{x}}[n]=[\varepsilon_r]^{1/2}\mathbf{x}[n] \qquad ,\\
&\overline{\mathbf{M}}=[\varepsilon_r]^{-1/2}\left[\frac{\Delta t^2}{\varepsilon_0 u_0}\nabla\times\nabla\times\right][\varepsilon_r]^{-1/2}
\end{aligned} \tag{3.33}$$

With this variation, $\overline{\mathbf{M}}$ is a real symmetric matrix which ensures that its eigenvectors form a complete set of the basis function in the solution space. The eigen-

analysis can then be carried out on (3.33) instead of (3.1) and $\overline{\mathbf{E}}$ is solved following the steps proposed in section III. Discrete Fourier Transform is performed on $\mathbf{E}$ via $\mathbf{E} = [\varepsilon_r]^{-1/2}\overline{\mathbf{E}}$ to find the resonance frequencies. The results are compared with the measured results [50, 51] and are presented in Table I for two different diameters of the dielectric rod. The results obtained with the two different methods show very good agreement, which verifies the proposed method.

Table 1 Comparison of the methods for resonant frequency of dielectric resonator.

Size		***Grids***	***Resonant Frequencies f(GHz)***		
2R (cm)	**t (cm)**		**Measured**	**FDTD method**	**Proposed method**
1.7551	0.5893	26×26×26	4.136	4.171	4.171
1.9228	0.6426	31×31×32	3.76	3.696	3.696

As a short summary, the four examples above verify that the proposed method provides the exact solution of the conventional FDTD method in a different solution path. The proposed method applies the eigen expansion of the discrete FDTD system and therefore its successful applications hinge on having an efficient and effective eigen-solver. Since a large portion of the eigenvalues and their associated eigenvectors represents high-frequency modes or unstable modes, they can be identified and removed because they do contribute accurate solutions as a result of inherent FDTD high numerical dispersion errors at high frequencies ; only a relatively small number of the eigenvalues of small values need to be found. In general, they account for 10%-20% of all the eigenvalues. Many efficient techniques have been developed to find these eigenvalues and their eigenvectors, such as the model-order-reduction technique described in [26] and the combined FDTD-trial-simulation and model-order-reduction technique presented in [47]. In our case, we use the one presented in [26] . We obtain the similar computational speedup of roughly six times in finding the needed eigenvalues and their associated modes in comparison with the conventional FDTD method at the same solution accuracy level.

3.7 TREATMENT OF ABSORBING BOUNDARY CONDITIONS (ABC)

The above numerical experiments are performed in a closed structure. In open structures, the absorbing boundary conditions (ABCs) are always needed to truncate the modeling domains while eliminating the reflections induced by the truncation. Among various absorbing boundary schemes, the perfectly-matched layers (PML) is considered to have the best performance of all and is widely used.

The extension or incorporation of the proposed analytical method to the absorbing boundary conditions including PML has been found non-trivial. It requires thorough analyses like those presented in the above again. We are currently working on it and expect to report the results in our future publications. Nevertheless, it is worth to mention that a straightforward and practical technique to deal with ABCs is to use the approach described in [26]: a solution domain is divided into the ABC regions and the main region containing the structures to be solved for. In the ABC (e.g., PML) regions, the fields are computed in the conventional FDTD manner. In the main region, the proposed method is applied but with the field values at the interface nodes between the two regions acting as soft sources.

Below are our initial formulations of the PMLs with the proposed analytical method. Take Berenger's field-split PML formulations [52, 53] for TE wave as an example. The governing equations in the PML region can be expressed as:

$$\begin{bmatrix} [\varepsilon_0] & & & \\ & [\varepsilon_0] & & \\ & & [u_0] & \\ & & & [u_0] \end{bmatrix} \frac{\partial}{\partial t} \begin{bmatrix} E_x \\ E_y \\ H_{zx} \\ H_{zy} \end{bmatrix} = \begin{bmatrix} [-\sigma_y] & & [\frac{\partial}{\partial y}] & [\frac{\partial}{\partial y}] \\ & [-\sigma_x] & [-\frac{\partial}{\partial x}] & [-\frac{\partial}{\partial x}] \\ & [-\frac{\partial}{\partial x}] & [-\sigma_{mx}] & \\ [\frac{\partial}{\partial y}] & & & [-\sigma_{my}] \end{bmatrix} \begin{bmatrix} E_x \\ E_y \\ H_{zx} \\ H_{zy} \end{bmatrix}. \quad (3.34)$$

The bracketed terms are the corresponding parameters in matrix form. (3.34) is much more complex than (2.2) because of the introduction of anisotropic and lossy terms in the PML formulations. It will lead to a generalized eigenvalue (GEV) system, $\lambda A\mathbf{x} = B\mathbf{x}$ (in which λ and $\mathbf{x}$ are generalized eigenvalues and eigenvectors of the

system). Once the stable eigenmodes(vectors) are solved, the similar results may be obtained.

An alternative approach to including the PML is to divide a problem domain into two regions: the PML region and the main region in which the structure to be studied is contained. Because the PML region is fictitious and should not contain information about the structure studied, the above described methods are only to the main region. In the PML region, simulation can be done with the conventional FDTD method. Interactions between the two regions occur at the interfacing nodes only. To the main region, the influences due to the PML region can be considered as the equivalent input sources at these interfacing nodes. In another word, soft sources are used to count for the PML interfaces.

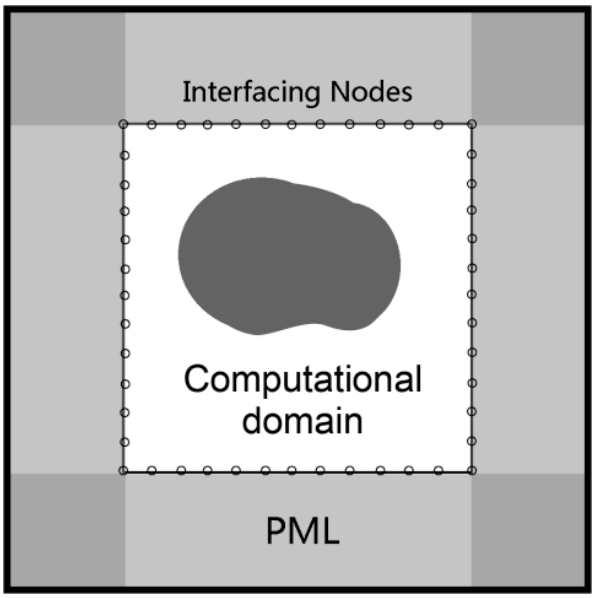

Figure 3.6 PML layers surrounds the computational domain; the circles represent the interfacing nodes.

More specifically, electrical field in the main region can be divided into

$$E[n] = \begin{bmatrix} E_m \\ E_i \end{bmatrix} \quad , \tag{3.35}$$

In which E_i are the fields at the interfacing nodes and the E_m represents the fields in the main region. The wave equation (3.1) can be applied to the main region directly, which is now written as

$$\begin{bmatrix} E_m[n+1] \\ E_i[n+1] \end{bmatrix} - 2\begin{bmatrix} E_m[n] \\ E_i[n] \end{bmatrix} + \begin{bmatrix} E_m[n-1] \\ E_i[n-1] \end{bmatrix} + M\begin{bmatrix} E_m[n] \\ E_i[n] \end{bmatrix} = x[n] , \quad (3.36)$$

$$M = \begin{bmatrix} M_{m-m} & M_{m-i} \\ M_{i-m} & M_{i-i} \end{bmatrix} , \quad (3.37)$$

in which matrix $M_{m\text{-}m}$, $M_{m\text{-}i}$, $M_{i\text{-}m}$, and $M_{i\text{-}i}$ are the sub-matrices of system matrix M for the main region, with sizes of E_m, E_i, respectively. Also, the field quantities at the interfacing nodes are involved in the calculations of the PML layer. The field values at the interfacing nodes due to PML can be considered as input sources (i.e. the soft source terms) in the field update process of the main region.

(3.36) can be expanded as

$$\begin{aligned} E_m[n+1] - 2E_m[n] + E_m[n-1] + M_{m-m}E_m[n] + M_{m-i}E_i[n] &= x_m[n] \\ E_m[n+1] - 2E_m[n] + E_m[n-1] + M_{m-m}E_m[n] &= x_m[n] - M_{m-i}E_i[n] \end{aligned} . \quad (3.38)$$

The final equation above has the form similar to equation (3.1) and (3.19). The fields in the main region can then be solved by the procedure described before. The influence from the PML region to the main region is contained in the term $-M_{m-i}E_i[n]$ and become part of the input source term. In reference [8], a similar absorbing treatment, which divides the whole region into a main computation region and a ABC region; they are then solved separately. Further work along this line is needed which is beyond the scope of this thesis due to the limitation of the time.

3.8 SUMMARY

In this chapter, based on the eigen analysis of the FDTD formulation, we have derived the analytical solutions for the FDTD method and re-analyzed the stability

condition of the FDTD method in terms of impulse responses. Based on our analyses, the numerical solution of the FDTD can be expanded in terms of spatially time-invariant eigenmodes with the time-varying expansion coefficients $a_{i,n}$. The iterative march-on-in-time process of the FDTD can be replaced by directly solving the expansion coefficient $a_{i,n}$. As a result, an alternative approach to solving the FDTD method is developed where the FDTD solution can be obtained at any time step without recursive march on time. This new approach allows the use of existing eigen solvers and may present time-saving in some cases where long simulation time is required. More significantly, the analytical forms of the FDTD solutions present the possibility of applications of advanced signal processing techniques as well as storing of structural impulse responses after pre-computing. Three preliminary numerical examples are given to verify the theory and the effectiveness of the proposed approach. The work opens another horizon in obtaining and using FDTD solutions.

CHAPTER 4 DEVELOPMENT OF EFFECTIVE TIME REVERSAL METHOD

4.1 INTRODUCTION

Source locating has been a topic of research and development in acoustic, electromagnetics and other areas. Various methods have been developed to locate sources in a time-invariant environment or domain. Many of them use the time-of-arrival or phase for the source locations, which may not necessarily use all the information in the full-wave received signals or fields. Environmental effects often interfere the locating process and degrade locating accuracy. The time reversal (TR) method [27, 28] has become a choice for source identifications in many applications. There are two steps with the time reversal technique: forward propagation (simulation) and backward propagation (simulation). In the forward propagation, signals, for example electromagnetic fields emitted by unknown sources, propagate and are then recorded at preselected output nodes of a domain. Then in the backward simulation, the recorded fields are reversed in time and re-injected back into the propagation domain for the same period. The field peaks will be formed and observed at the end of the reversed signal propagation and they indicate the original source locations.

Robust and simple to implement, the TR methods have drawn much attention recently. For example, [27, 28] apply TR for acoustic analysis; [54] uses the TR technique to locate earthquake sources. [29, 30, 32, 55] apply the TR process to electromagnetic source locations.

With a conventional source locating technique, multipath is considered as an adverse effect against the location accuracy. The time reversal is the technique which can utilize the multipath for performance improvements for target detection and/or source localization. It exploits the reciprocity of the propagation medium and the time-reversal invariant natural of the wave equation for field focusing. It processes the multipath copies of the transmitted signals in the medium, as induced by reflection, refraction and multiple scatterings, in a constructive manner, resulting in the improvement of the focusing resolution. The time reversal technique has successfully been applied and its capability has been demonstrated [27-32][54-55]. Since then, the time-reversal methods have also been applied to electromagnetic structures. The wide-range applications have spurred

extensive research in this area. The work presented in this thesis focuses on the time-reversal methods with time-domain electromagnetic modeling.

Figure 4.1 shows a typical computational time reversal simulation employing the FDTD method. The problem domain under consideration is a cavity which provides a multipath-rich environment. Figure 4.1a & 4.1b shows the source excitation and the field propagation within the cavity in the forward propagation. The fields are then recorded at the selected output nodes for a given length of time (or a fixed number of time steps). They are then re-injected into the cavity at the output locations. Figure 4.1c shows the recorded fields that are re-injected back into the cavity. The re-injected fields will then propagate back into the cavity and produce a time response at every node in the FDTD grid, including at the original source nodes. This is the reverse or backward simulation process. If the duration of the backward propagation is the same as that of the forward propagation, the fields will generally form maxima at the original source nodes and the locations of the sources are identified. Figure 4.1d shows the results of the time reversal process in which the source is identified by the field peak.

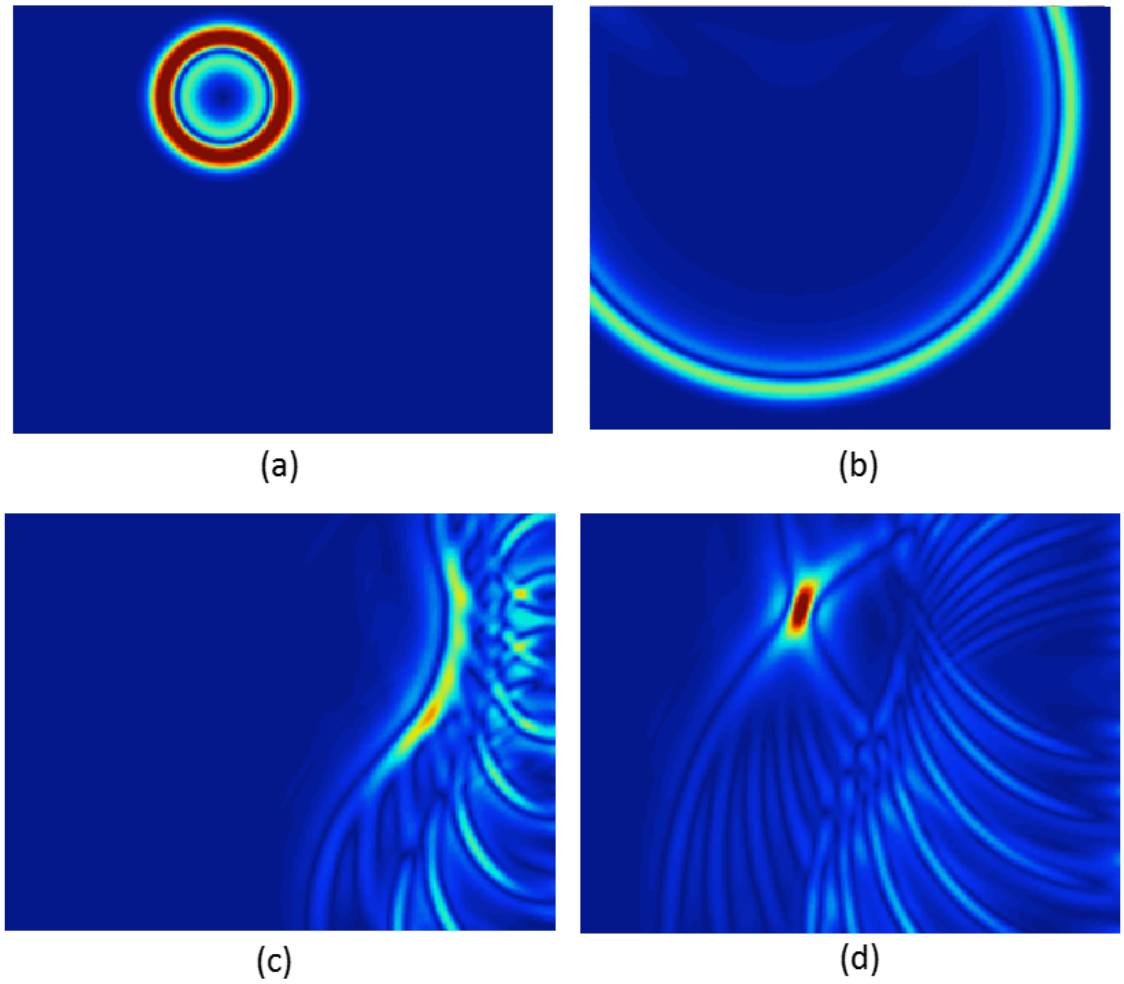

Figure 4.1 A typical time reversal process: (a) forward fields excited by a point sources; (b) wave propagation within the cavity and recorded at the output nodes; (c) re-injection of the recorded fields that are time-reversed at the output nodes; (d) re-focusing of the fields at the original source nodes at the end of the backward propagation.

The figure above shows good focusing effect at the original source location with the time reversal; the sources location can be identified easily. There are issues with the conventional time reversal method. First, sources are simply located by peak identification. In the following sections, it can be shown by examples and in theory that the peak values may not always present the true locations of the sources. when multiple sources exist simultaneously, interference may occur among the signals excited by these sources, leading to complexity and challenges in peak identification and locating.

Secondly, in the simulations so far, full-spectrum impulses are considered. In practice, only limited-band of the recorded signals are available by measurements. Therefore, it is much desirable to develop a TR method that accommodate the signals of limited-bands. The motivation of the work presented in the following sections is to address the above two issues and develop new methods and techniques whenever proper and needed.

4.2 The Location Condition for Reconstruction of Multiple Sources Using Time Reversal Method

4.2.1 Theoretic Analysis of The Conventional Time Reversal Method

In this section, without loss of generality, theoretical analysis of a typical computational time reversal is performed. Then, an ergodic air-filled cavity bounded by perfectly electric conductors (PECs) [33, 56] is considered as a numerical example and the finite-difference time-domain (FDTD) method is employed for simulations. Within the cavity, multiple source and output (or receiver) nodes are chosen and an electric field impulse excitation is applied at the source nodes.

First, we consider the forward propagation (simulation). Suppose that J single impulse excitations $x_j(n)$ are injected into the cavity at J source nodes. Mathematically, they can be expressed as:

$$x_j[n] = a_j \delta[n], \quad j = 1,...,J. \tag{4.1}$$

a_j is the amplitude of the impulse injected at the j-th source node at the time step n. δ is the Kronecker or unit impulse function and n is the time index or time step with the total number of time steps being N.

Now consider I preselected output (or receiver) nodes. The signals or fields recorded at each of them can then be expressed as:

$$y_i[n] = \sum_{j=1}^{J} a_j h_{ij}[n], \ i = 1,...,I, \ n = 0,1,...,N-1. \tag{4.2}$$

where $h_{ij}[n]$is the impulse response recorded at the *i*-th output node due to the unit impulse excitation at the *j*-th source node. If the transmission line matrix (TLM) method is applied, $h_{ij}[n]$ is defined as an element of the Johns matrix [57, 58].

Assume that the propagation medium is reciprocal. The response at the *i*-th node due to the unit impulse excitation at the *j*-th node is then the same as the response at the *j*-th node due to the unit impulse excitation at the *i*-th node.

In the subsequent backward propagation, the field responses described by (4.2) that were recorded at the *i*-th node, are reversed in time:

$$y_i^r[n] = y_i[N-1-n] = \sum_{j=1}^{J} a_j h_{ij}[N-1-n]. \tag{4.3}$$

This inverse response, when re-injected into the problem domain at the *i*-th output node, produces the following output at the *j*-th source node:

$$\begin{aligned} S_j^{\,i}[n] &= h_{ji}[n] \otimes y_i^r[n] = h_{ij}[n] \otimes y_i^r[n] \\ &= \sum_{m=0}^{n} h_{ij}[m] y_i^r[n-m], \quad n = 0 \ldots N\text{-}1 \end{aligned} . \tag{4.4}$$

The total fields or signals at the *j*-th source node will be the sum of the responses due to the re-injections at all the output nodes:

$$\begin{aligned} S_j[n] &= \sum_{i=1}^{I} S_j^{\,i}[n] = \sum_{i=1}^{I} \sum_{m=0}^{n} h_{ij}[m] y_i^r[n-m] \\ &= \sum_{i=1}^{I} \sum_{m=0}^{n} h_{ij}[m] \sum_{j'=1}^{J} a_{j'} h_{ij'}[N-1-n+m] \\ &= \sum_{i=1}^{I} \sum_{j'=1}^{J} \sum_{m=0}^{n} h_{ij}[m] a_{j'} h_{ij'}[N-1-n+m] \\ &= \sum_{j=1}^{J} \sum_{j'=1}^{I} a_{j'} \left(\sum_{m=0}^{n} h_{ij}[m] h_{ij'}[N-1-n+m] \right) \end{aligned} . \tag{4.5}$$

in which *m*=0,..,*N*-1 is the dummy time index for the convolutional shift of time instances. j' is the index of source nodes which we have introduced to distinguish it from operations involving the index *j*.

At the last step of the backward propagation, i.e. $n = N$-1, (4.5) becomes

$$S_j[N-1] = \sum_{i=1}^{I}\sum_{j'=1}^{J} a_{j'}\left(\sum_{m=0}^{N-1} h_{ij}[m]h_{ij'}[N-1-N+1+m]\right)$$

$$= \sum_{i=1,\, j=j'}^{I} a_j\left(\sum_{m=0}^{N-1} h_{ij}[m]h_{ij}[m]\right) + \sum_{i=1}^{I}\sum_{j'=1,\, j'\neq j}^{J} a_{j'}\left(\sum_{m=0}^{N-1} h_{ij}[m]h_{ij'}[m]\right). \quad (4.6)$$

$$= \sum_{i=1}^{I} a_j R_{h_{ij}h_{ij}}[0] + \sum_{i=1}^{I}\sum_{j'=1,\, j'\neq j}^{J} a_{i'}\left(\sum_{m=0}^{N-1} h_{ij}[m]h_{ij'}[m]\right)$$

The first term in the right-hand side (RHS) of (4.6),

$$R_{h_{ij}h_{ij}}[0] = \sum_{m=0}^{N-1} h_{ij}[m]h_{ij}[m] = \sum_{m=0}^{N-1} h_{ij}^{\,2}[m] \geq 0 \quad , \quad (4.7)$$

is the aggregation of auto-correlation of $h_{ji}[n]$ which tends to have a relatively large value; it leads to the spatial and temporal field focusing or peak at the j-th source location.

The second term in the RHS of (4.6) is a summation of cross-correlated terms generated by different sources. It represents the response recorded at one source caused by other sources from the forward and backward propagation. Since these signals are not correlated, the second term has in general a relatively low value in comparison with the first term. Therefore, (4.6) is in general dominated by the first term and will present large values at the original source locations. Then, the usual way to identify the source node locations (or to reconstruct the sources) is to find the highest peaks at the final time of the backward propagation.

In the above analysis, we assume that all $h_{ji}[n]$ are different from each other so that the auto-correlation occurs only at the original source location j. For the case without ergodic property, false peaks can also arise due to degenerescence of the field response or symmetries. $h_{ji}[n]$ can be the same for different values of j and the reconstruction yields peaks at all those false positions.

Even in the ergodic cases, sometimes, the second terms or cross terms of (4.6) may still become large, destroy the field focusing, and interfere with the above peak identification process; in other words, the auto-correlation terms may not be sufficiently large to be clearly identifiable. In such a situation, the source reconstruction may fail if one relies only on the identification of the peak values.

To illustrate the unsuccessful case, experiments are performed on the cavity as shown in Figure 4.2. As seen, the sources are difficult to identify due to the false peaks resulting from the large uncorrelated terms at non-source locations (or due to insufficient magnitude of the peaks at the original source locations). The source reconstruction does not work in this case. This phenomenon is also found in certain cases modeled by TLM method.

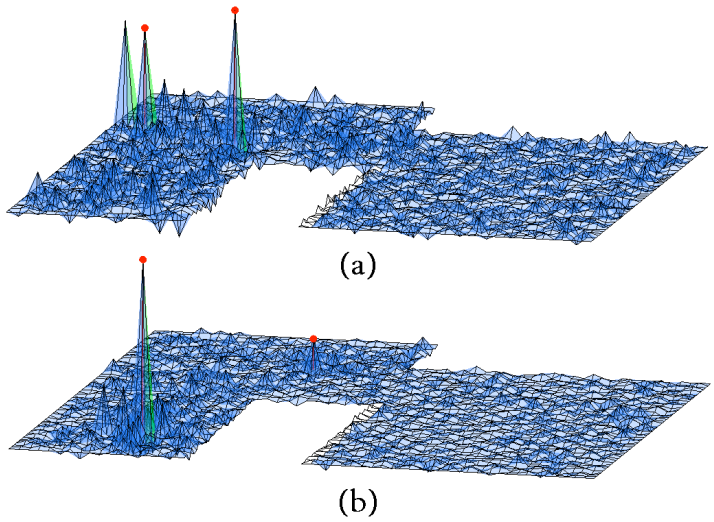

Figure 4.2 Two cases in which the reconstruction of sources with the time reversal method is unsuccessful. (a) The two original source amplitudes (with red dots) are equal. A peak is found at a source-free location. (b)The two original source amplitudes are 1 and 0.3 (with red dots). The source of amplitude 0.3 cannot be identified unambiguously.

In the next section, following up on the above analysis, we derive a quantitative condition for the exact identification of the source node locations even when the peak identification approach fails, or the field focusing does not occur. The condition requires neither the knowledge of the propagation environment nor the identification of field peaks.

4.2.2 The Condition for Reconstruction of Multiple Sources

In this section, we derive a mathematical condition for the accurate identification of multiple source-node locations.

First, we sum the squares of the field response samples (i.e. (4.2)) recorded at the *i*-th output node during the forward propagation:

$$\begin{aligned}\sum_{n=0}^{N-1} y_i^{\,2}[n] &= \sum_{n=0}^{N-1}\Big(\sum_{j=1}^{J} a_j h_{ij}[n]\Big)^2 \\ &= \sum_{n=0}^{N-1}\Big(\sum_{j=1}^{J}\sum_{j'=1}^{J} a_j a_{j'} h_{ij}[n] h_{ij'}[n]\Big)\end{aligned} \quad . \tag{4.8}$$

Then, unlike in the backward propagation of the conventional time-reversal method where the time-reversed fields or signals recorded are rejected into the problem domain at all the output nodes simultaneously, we perform *I* separate backward propagations. During each simulation we re-inject only a single time-reversed response into a single output node, say the *i*-th node, at which that response has been recorded; we denote the process as the *i*-th backward propagations. At the final time step of the *i*-th backward transmission i.e. *n*=*N*-1, the field response at the *j*-th source is:

$$\begin{aligned} S_j^i[N-1] &= S_j^i[n]\big|_{n=N-1} = \big(h_{ji}[n] \otimes y_i^r[n]\big)\big|_{n=N-1} \\ &= \Big(h_{ij}[n] \otimes \sum_{j'=1}^{J} a_{j'} h_{ij'}[N-1-n]\Big)\Big|_{n=N-1} \\ &= \Big(h_{ij}[n] \otimes \sum_{j'=1}^{J} a_{j'} h_{ij'}[N-1-n]\Big)\Big|_{n=N-1} \\ &= \sum_{m=0}^{N-1} h_{ij}[m] \sum_{j'=1}^{J} a_{j'} h_{ij'}[m] \\ &= \sum_{m=0}^{N-1} h_{ij}[m] y_i[m] \end{aligned} \quad . \tag{4.9}$$

By comparing (4.8) and (4.9), we find that

$$\sum_{n=0}^{N-1} y_i^{\,2}[n] = \sum_{j=1}^{J} a_j S_j^i[N-1] \ . \tag{4.10}$$

(4.10) establishes the relationship between the energy of received signal y_i[n] (which is reversed and re-transmitted) with the final state value at the sources in the backward propagation. Now we now reformulate (4.10) as:

$$\sum_{j=1}^{J} a_j \overline{S}_j^i = 1, \quad \text{in which } \overline{S}_j^i = \frac{S_j^i[N-1]}{\sum_{n=0}^{N-1} y_i^2[n]}. \tag{4.11}$$

The condition (4.11) must be satisfied at each source location. In fact, $\sum_{n=0}^{N-1} y_i^2[n]$ is the total signal energy received or recorded at the *i*-th output node during the forward propagation. $S_j^i[N-1]$ is the magnitude of the signal recorded at the *j*-th source location at the last time step of the *i*-th backward propagation.

4.2.3 Verification of the Condition

A numerical experiment was performed to verify the condition (4.11). Without loss of generality, the FDTD method is applied to simulate a PEC ergodic cavity with two sources and three output locations (i.e., *J*=2 and *I*=3). The amplitudes of the two sources are chosen to be 0.2 and 1, respectively.

First, the forward propagation is run and electric field values or signals are recorded at each output node. The signals are time-reversed. Then three separate backward propagations are run and in each of them, only one of the three output nodes is excited with the time-reversed signal it has recorded. The field distribution at the end of each backward propagation is recorded.

After the backward propagations, we check whether condition (4.11) is satisfied for any group of two nodes in the solution domain. If one of the groups does satisfy (4.11), it will represent the actual sources.

More specifically, we randomly group the nodes into pairs and check if the following condition is satisfied for all *j*:

$$a_1 \overline{S}_1^j + a_2 \overline{S}_2^j = 1. \tag{4.12}$$

j=1, 2 and 3 represent the backward transmissions with the time-reversed signals re-injected into each of the 3 output locations, respectively.

In reality, checking condition (4.12) can be made equivalent and easy by examining whether the determinant of matrix (4.13) below is zero. If the determinant is zero, the condition is satisfied and the source locations are found.

$$\begin{bmatrix} \overline{S}^1_1 & \overline{S}^1_2 & -1 \\ \overline{S}^2_1 & \overline{S}^2_2 & -1 \\ \overline{S}^3_1 & \overline{S}^3_2 & -1 \end{bmatrix}. \tag{4.13}$$

Figure 4.3 shows the determinant values of (4.13) for 10,000 pair group of source candidates. It appears that only one group among these 10,000 yields a determinant that is significantly smaller than all the others by about eight orders of magnitude. This particular group turns out to correspond to the original source locations used in the forward propagation. Once the sources are correctly located, their amplitudes are easily solved with equation (12).

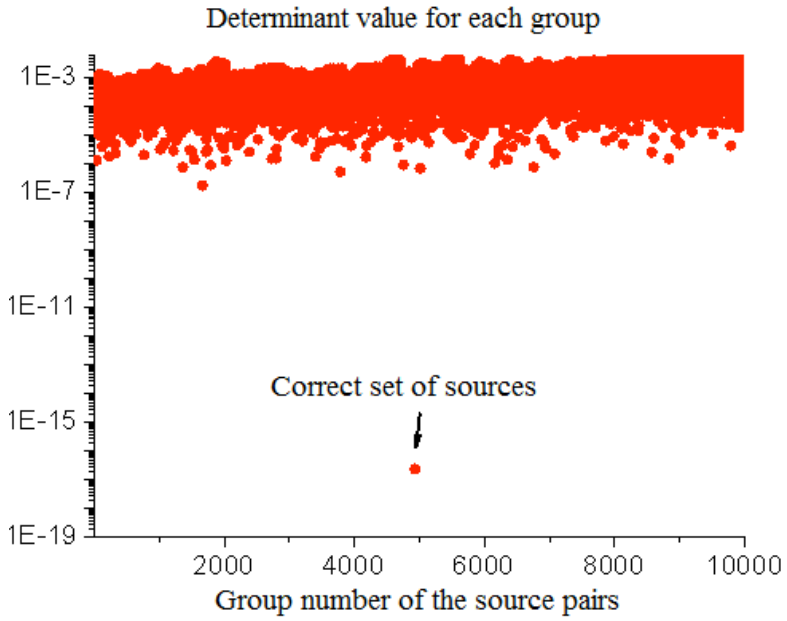

Figure 4.3 Determinant of matrix (4.13) for 10000 groups of two nodes. Among them only the determinant of one group has a very small value close to zero. This group turns out to be the correct pair of source node.

4.3 Application of The Condition For Reconstruction Of Multiple Sources

4.3.1 The Proposed Method to Find the Source Locations

In the above example, we assume that we have a prior knowledge of the number of the sources being two. In practice, however, it is not known. A sequential trial-and-error approach can be employed to apply the condition to source reconstruction. More specifically, we may first start to assume the number of the sources to be 1 and perform the test described above; if the condition is satisfied, the source location is found. If not, we then assume the number of the sources is 2 and perform the test, and so on. In theory, this approach will allow us to find the source locations. In reality, however, its computational expense will be prohibitive, especially for an electrically large structure. Hence, an efficient method is desired to apply the condition for source reconstruction. In the following paragraphs, we propose the regularized least square (RLS) method .

Assume M locations as the possible source locations. Based on the condition (4.10), consider that at non-source locations the amplitudes should be 0; that is, (4.10) can be rewritten as a condition that amplitudes of all these assumed M sources must satisfy:

$$\begin{bmatrix} S_1^{\,1} & \cdots & S_M^{\,1} \\ \cdots & \cdots & \cdots \\ S_1^{\,I} & \cdots & S_M^{\,I} \end{bmatrix}_{I*M} \begin{bmatrix} a_1 \\ \\ \cdots \\ \\ a_M \end{bmatrix}_{M*1} = \begin{bmatrix} \sum_{n=0}^{N-1} y_1^{\,2}[n] \\ \cdots \\ \sum_{n=0}^{N-1} y_I^{\,2}[n] \end{bmatrix}_{I*1}, \qquad (4.14)$$

where the element $S_m^{\,i}$ is the field value recorded at the assumed m-th source location at the end of the i-th backward transmission. a_m, m=1…M, is the amplitude of the impulse excitation at the assumed m-th source location.

Since a_m is the amplitude of the impulse excitation at the source location, it will have a non-zero value at a true source location and zero at all other non-source locations.

In other words, the exact solutions of (4.14) can automatically yield true source locations and remove the non-source locations by identifying non-zero elements of $[a_m]$.

Equation (4.14) represents I equations with M unknowns. Usually, M is much larger than I. Hence the equation is underdetermined. It can then be solved in the least square (LS) manner. Moreover, the smallest number of non-zero elements a_m is the constraint to the LS system, leading to a regularized least square (RLS) formulation, i.e. the solution a_m is sparse. To find the sparse solution, a L-1 regularization term is added to the underdetermined equation. The formulation can then be expressed as:

$$\text{minimize } \left(\left\| [S][a] - \left[\sum_{n=1}^{N} y_j{}^2[n] \right] \right\|^2 + \lambda |a| \right) \tag{4.15}$$

in which λ is the regularization factor chosen empirically. The constraint equation (4.15) is to find the sparsest solution vector, which can be solved numerically by applying a solution algorithm such as LASSO [59-61]. The resulting amplitude coefficients $[a_m]$ that are non-zero identify the source locations.

4.3.2 Numerical Experiment with the Proposed RLS Method

In the following numerical example, we choose three source nodes and six output nodes within the cavity domain. We then apply the proposed RLS method by selecting 1500 nodes within an area that is assumed to contain the three source nodes. M is thus equal to 1500. Using the algorithm described in [59], we compute the amplitudes a_j; the value of the regularization factor λ is chosen empirically to be between 0.001 and 0.02. The optimal choice of λ is a subject of future research. The results of the computation are shown in Figure 4.4.

As can be seen, at only three node locations, a_j is non-zero; they turn out to be the correct source locations. The computed source amplitudes are also close to the true values. If needed, the exact amplitudes can be found by solving (10) for the identified source locations. Therefore, this example proves the effectiveness of the proposed method.

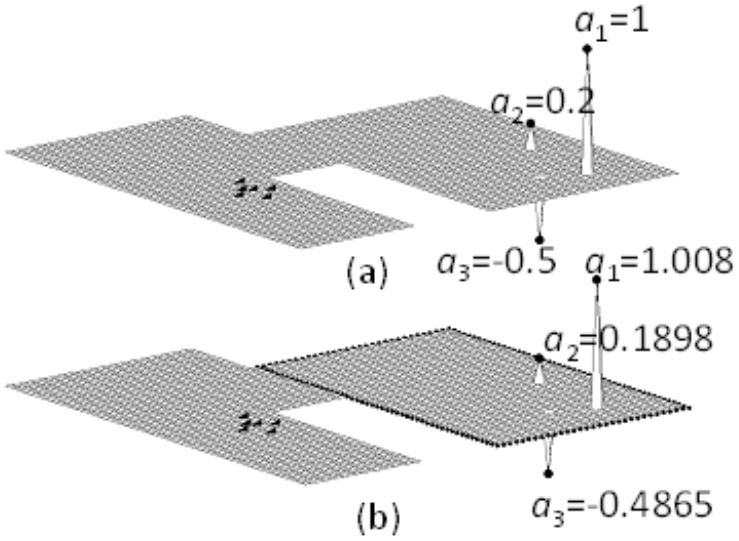

Figure 4.4 Result of source reconstructions with the proposed method. The dots in the left region of the problem domain indicate the eight output nodes. The sources are shown as the peaks. (a) shows the original source locations and their amplitudes. (b) presents the results obtained with the RLS method.

As a summary of this section, we have first developed a condition for reconstruction of multiple sources. It is verified by the numerical experiments. The condition can be used as a validation of the possible sources identified. In other words, when we identify the sources using the conventional time reversal process, the condition can be used as a test to see if the sources identified are indeed true. Next, based on the proposed condition, we have developed a RLS scheme to directly calculate the possible source locations by solving the underdetermined equation. The result shows the effectiveness and reliability of the proposed method even in the cases that the conventional time reversal has difficulty in identifying all sources.

4.4 Source Reconstruction With Realistic Band-Limited Frequency Domain Signals

We have so far used time domain impulse responses of infinitely large frequency band, which yield high spatial resolutions. However, in realistic situations, the field responses at output nodes are often measured or recorded in frequency domain within a

limited frequency band. Direct application of regular frequency-to-time transformation techniques, e.g. inverse Fourier transform, to convert these band-limited frequency-domain field responses into their time domain counterparts, most likely lead to non-causal complex time-domain signals; they cannot be used in the time reversal process. Therefore, it is necessary to develop a method to extract causal time-domain responses from band-limited frequency domain measurements so they can be used for the time reversal source reconstruction. In the following subsections, we develop an extraction method specifically for the time-reversal method.

4.4.1 Reconstruction of Fields from Band-Limited Frequency Domain Responses or Measurements

To better explain the method, we use again the numerical experiment of the ergodic cavity of Figure 4.2 and Figure 4.4. The frequency domain signals at the output nodes is first obtained by the discrete Fourier transform (DFT) of the time-domain responses recorded at the pre-selected output nodes. At the *i*-th output node, the recorded time-domain signal or field is expressed by (4.2). Its frequency domain correspondent is

$$Y_i[k] = DFT(y_i[n]), \quad k = 0,1,2,...,N-1 \tag{4.16}$$

where *DFT* is the discrete Fourier transform, k is the frequency step index which represents the frequency point of $k\Delta f = k / \Delta t$ with Δt being the FDTD time step.

To emulate the band-limited field responses, we remove the frequency contents outside a preselected frequency band of $[k_l \Delta f, k_h \Delta f]$ such that the following band-limited response is used now for the time reversal source reconstructions:

$$Y_i^c[k] = \begin{cases} Y_i[k], \omega \in [k_l, k_h] \\ 0, \qquad \omega \notin [k_l, k_h] \end{cases}. \tag{4.17}$$

The graphical representations of the band-limited responses (4.17) are shown in Figure 4.5.

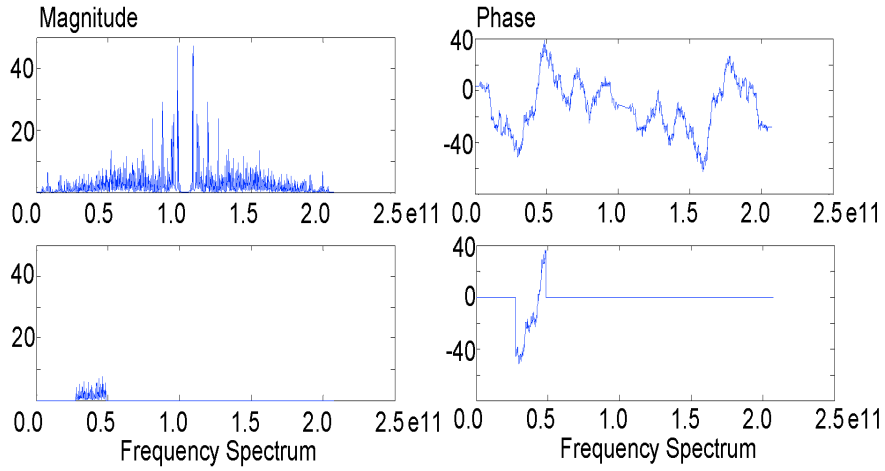

Figure 4.5 Creation of the band-limited frequency domain fields. The top two figures are the magnitude and phase of the frequency-domain fields recorded in a full spectrum. The bottom two figures show the band-limited spectrum that results from the removal of the contents outside the preselected frequency band of [k_l, k_h].

If the inverse Fourier transform is directly applied to (4.17) (which represents the band-limited signals), the resulting time domain response becomes complex and non-causal; hence, it cannot be used in the time reversal process.

To construct the usable time domain equivalent response, we propose to approximate the band-limited response as follows:

$$y_i^c[n] = \sum_{k=k_l}^{k_h} \left| Y_i^c(k) \right| \cos\left(2\pi n \frac{k}{N} + \angle Y_i^c(k)\right), \quad n = 0,1,2,\ldots,N-1. \tag{4.18}$$

It is a summation of monochromatic cosine functions. Each cosine function has a frequency of $k\Delta f = k / \Delta t$, an amplitude of $|Y_j^c(k)|$ and a phase $\angle Y_i^c(k)$, respectively. (4.18) is a real time-domain sequence.

By taking the *DFT* of (4.18), we can show that it has exactly the same values as $Y_i[k]$ within the band of interest $[k_l \Delta f, k_h \Delta f]$. Figure 4.6 shows the time and frequency domain representation of (4.18) and compares it to the original time response (4.16).

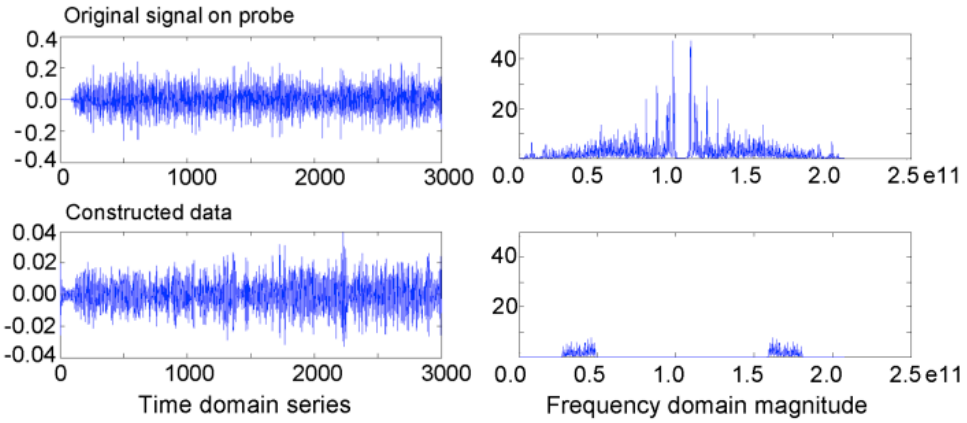

Figure 4.6 Comparison between original and the reconstructed time responses. The two figures on the left are the time-domain signals and the figures on the right are the frequency domain signals. The top two figures show the original responses, and the bottom two figures show the responses reconstructed with (4.18).

After (4.18) is computed for each output node, it is time-reversed and re-injected into the cavity, and the backward simulation is run by following the procedure described in Section II. At the final step of the backward simulation, the field distribution shows clear peaks within the structure as Figure 4.7 shows.

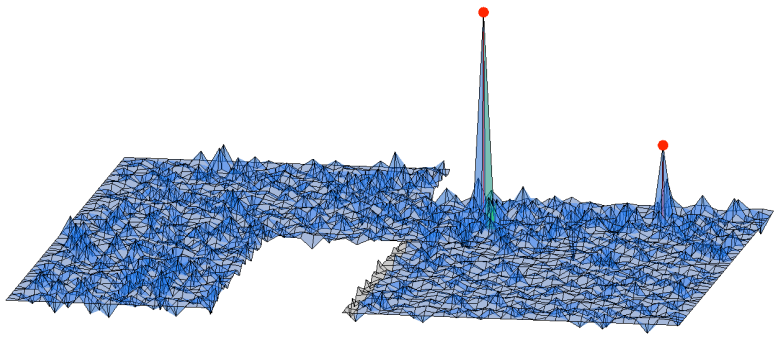

Figure 4.7 Sources reconstructed from band-limited responses, yielding well-defined peaks at the original source nodes.

More numerical experiments were performed with different choices of sources and output nodes as well as different limited frequency bands. The results are all similar and unambiguous. The reason can be theoretically explained as follows.

Similar to (4.9), the response $S_j^i[N-1]$ at the *j*-th source location at the end of the *i*-th backward simulation is:

$$S_j^i[N-1] = \sum_{n=0}^{N-1} h_{ij}[n] y_i^c[n] \tag{4.19}$$

(4.19) shows that the final state value of backward transmission is the correlation product of constructed signal and the corresponding impulse response. On the other hand, based on Plancherel theorem, the correlation product of the time domain signals is equivalent to their conjugate-complex multiplication in frequency domain. That is,

$$\sum_{n=0}^{N-1} h_{ij}[n] y_i{}^c[n] = \frac{1}{N} \sum_{k=0}^{N-1} H_{ij}[k] (Y_i^c[k])^* \quad . \tag{4.20}$$

where

$$\begin{aligned} H_{ij}[k] &= DFT(h_{ij}[n]) \ , \\ Y_i^c[k] &= DFT(y_i^c[n]) \ . \end{aligned} \tag{4.21}$$

After further manipulation, we have

$$\begin{aligned} S_i{}^j[N-1] &= \frac{1}{N} \sum_{k=0}^{N-1} H_{ij}[k] \sum_{j'} a_{j'} (H_{ij'}^c[k])^* \\ &= \frac{1}{N} \sum_{k=k_l, j=j'}^{k_h} a_j \left| H_{ij}[k] \right|^2 + \frac{1}{N} \sum_{j', j \neq j'}^{J} \sum_{k=k_l}^{k_h} a_{j'} H_{ij}[k] H_{ij'}{}^*[k] \end{aligned} \tag{4.22}$$

The first term on the right-hand side is the summation of the positive numbers which aggregate and form a peak value. The second terms of the right-hand side represent the cross-terms between different sources and they will not accumulate constructively in most cases; therefore, they do not interfere with the peak values. Since the addition of the first term only takes place at the source nodes, focusing occurs at the source locations, very much like what is described for conventional TR focusing in Section 4.3.

In short, (4.22) provides the theoretical foundation for the proposed method in which a band-limited response is used to reconstruct its sources with the time-reversal method.

4.4.2 The Condition for Source Reconstruction from Band-Limited Field Responses

In the previous sections, we propose a method to reconstruct sources from band-limited field responses via time-reversal and field peak identification. Like that described in Section II, the method should work most of the time but may fail in some special cases. Here we derive the source locating condition that does not require the peak identifications for the source locations with the band-limited responses.

From (4.19) we have

$$\begin{aligned} S_j^i[N-1] &= \sum_{n=0}^{N-1} h_{ij}[n] y_i^{\,c}[n] \\ \sum_{j=1}^{J} a_j S_j^i[N-1] &= \sum_{j=1}^{J} a_j \sum_{n=0}^{N-1} h_{ij}[n] y_i^{\,c}[n] \\ &= \sum_{n=0}^{N-1} \sum_{j=1}^{J} a_j h_{ij}[n] y_i^{\,c}[n] \\ &= \sum_{n=0}^{N-1} y_i[n] y_i^{\,c}[n] \end{aligned} \quad , \tag{4.23}$$

in which $S_j^i[N\text{-}1]$ is the field response recorded at the j-th source node, at the end of the i-th backward simulation during which the received signal at the i-th output node is reversed and re-injected into the domain at the i-th output node.

From our previous analysis, we have

$$\sum_{n=0}^{N-1} y_i[n] y_i^{\,c}[n] = \frac{1}{N} \sum_{k=0}^{N-1} Y_i[k] Y^*{}_i^{\,c}[k] \tag{4.24}$$

where $Y_i^c[k]$ is defined by (4.17).

From the band-limited property of $Y_i^c[k]$, we can get

$$\frac{1}{N} \sum_{k=0}^{N-1} Y_i[k] Y^*{}_i^{\,c}[k] = \frac{1}{N} \sum_{k=0}^{N-1} \left| Y_i^c[k] \right|^2 = \sum_{n=0}^{N-1} y_i^{\,c}[n]^2 \tag{4.25}$$

The last equality in the above equation is obtained with Paserval's theory.

From (4.24) and (4.25),

$$\sum_{n=0}^{N-1} y_i[n] y_i^c[n] = \sum_{n=0}^{N-1} y_i^c[n]^2 \quad . \tag{4.26}$$

Based on (4.23) and (4.26), we reach

$$\sum_{n=0}^{N-1} y_i^c[n]^2 = \sum_{j=1}^{J} a_j S_j^i[N-1] \tag{4.27}$$

Similar to (4.10), (4.27) shows the relationship between the energy of transmitted signal and final state value at source locations in the backward propagation. The only difference with (4.10) is that here we use the constructed signal $y_i^c[n]$ in the backward propagation. (4.27) establishes the condition for the band-limited fields that permit the locating of the sources without identification of field peaks.

4.4.3 The RLS Method with the Band-limited Field Responses

Following the procedure used in section II, the underdetermined equation is constructed based on (4.27) and solved with the RLS process and the constraint of minimum non-zero number of coefficients a_j.

A numerical example with four sources and eight output nodes has been computed, with M=1500 selected. The results are shown in Figure 4.8. It is seen that the sources are reconstructed exactly at their original locations, and their amplitudes are very close to the original values.

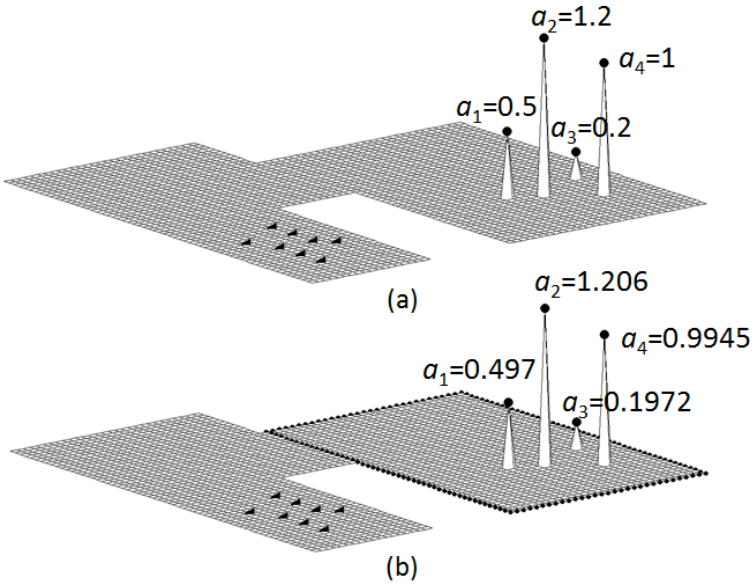

Figure 4.8 Source reconstruction from the band-limited field responses by applying the source locating condition (4.27). The locations of the eight output nodes are indicated by the dots in the left region of the problem domain. The sources are identified by the peaks. (a) shows the original sources, (b) shows the reconstructed sources. The rectangular boxed area is the domain where M=1500 nodes are used as source location candidates for setting up the underdetermined system for source reconstructions.

The above analysis and numerical experiments demonstrate that the proposed method to reconstruct impulsive sources from band-limited responses is viable. It makes the proposed time-reversal method applicable to real-world problems.

4.5 SUMMARY

In this chapter, we present a theoretical analysis of source reconstruction using the time reversal method with numerical methods like FDTD. We also develop a necessary condition for reconstructing multiple source locations and verify it with both theoretical analysis and numerical experiments. The condition does not involve Green's functions or identification of field peak values. Furthermore, we develop a method to process the band-limited fields or signals available in reality so that they can be used with the time reversal technique for multiple source reconstructions. Again, theoretical analysis and numerical experiments are provided to support and verify the method.

The implementation of the condition is also reported. After turning the condition into underdetermined equations, the L1-constrained MLS (Minimum Least Square) algorithm can be applied to derive acceptable result, identifies multiples sources or greatly reduce the number of the possible candidates. The proposed method does not involve solving for the complete system's impulse responses or Green functions; therefore, simplicity and robustness of the conventional TR method are retained.

CHAPTER 5 CONCLUSION

5.1 CONCLUDING REMARKS

This thesis has studied the finite-difference time-domain (FDTD) method for electromagnetic field modelling and its application in time reversal technique.

The FDTD method is the most widely used time-domain numerical method for electromagnetic modeling and simulations due to its algorithmic simplicity and flexibility. It has been extensively studied and applied for the past 40 years. However, much research has still been focused on improving the FDTD computational efficiency. One of the efforts is to break the restriction of the CFL limit and improve the computational speed since the FDTD method an explicit iterative march-on-time scheme. In this thesis, we have re-analyzed the stability condition of the FDTD method in terms of impulse responses using the based on the eigen analysis of the FDTD formulation. We show that the root cause of the instability of The FDTD method is the high-frequency eigenmodes whose eigenvalue is larger than 4. Since the eigenmodes are orthogonal, the unstable modes are of those with eigenvalues can be discarded, making the FDTD solutions stable. It is also found that the CFL condition does not always guarantee the stability of The FDTD method, which has not been seen in research reports so far.

By expanding the FDTD formulation in terms of the eigenmodes of the coefficient matrix of the spatially and temporally discretized system, the conventional march-on-time formulations are turned into solving the expansion coefficients. We have developed the recursive discrete system equations for the expansion coefficients. By solving the discrete system equation, analytical FDTD solutions are obtained. As a result, an alternative approach to the FDTD solution of an electromagnetic system is developed where the analytical FDTD solution can presents values at any time step without recursive march on time. Although finding the eigenmodes of the FDTD solutions may require computational efforts, they embody the full features of the FDTD systems once obtained. In addition, they can be stored and re-used without repeating the whole

simulation process again. Finally, because the unstable modes have been removed, there will be no issues that are related to the CFL stability limit.

The computational time reversal method utilizes the time-domain numerical methods to solve the inverse problem of source reconstructions. Without explicit quantifications of the multipath effects, source locations can be recovered through backward propagation of the time-reversed field signals of the forward simulations that are recorded at the preselected output locations. Simple and robust, the time reversal techniques have gained quiet interest and has been extensively studied and investigated. However, there are challenges and issues that need to be addressed for practical applications. In this thesis, we have addressed some of the challenges: we have derived a condition that enables precise reconstruction of multiple sources without false solutions. Based on the condition, we have developed the regularized least square (RLS) method that turns the time reversal method into an optimization formulation which could accurately recover the correct source locations, making the time-reversal available for practical uses.

To further improve the practicality of the time reversal method, we have developed a method that makes band-limited field signals applicable to the time reversal method. It extracts the time domain signals feasible for uses with the time reversal method from the band-limited field signals through simple expansions. The reconstructed signals work just like the full frequency-band signals that lead to spatial and temporal focusing at the original sources. We have further developed the time reversal process that incorporates the location condition proposed above, greatly extending the applications of time reversal method.

5.2 RECOMMENDATION FOR THE FUTURE WORK

The work of this thesis is original and opening new dimensions for both the time-domain numerical methods and the time reversal techniques. Therefore, there are many aspects of the topics can be further explored and developed. Due to the time limit of this thesis, they cannot be all covered. Here we present our thoughts for the future work in the hope that more work can be done in advancing the state-of-the-art based on the work presented in thesis.

The first recommendation is to apply our analysis to other time-domain methods. For example, the TLM method and RPIM (radial point interpolation meshless) method all have similar form as FDTD does: the system can be described as matrix, the solution is derived iteratively in the march-on-time manner. Hence the instability issue in these methods can be treated in the same way developed in this thesis.

The second recommendation is to develop the analytic FDTD solutions in complicated medium such as the PML region. The analytic FDTD solution in the PML region can greatly extend the analytic approach to open problems such as antennas and field scattering problems.

The third recommendation is to extend the analytical approach to structure design and optimization. For example, to design a waveguide filter with desired resonant frequencies, the conventional method will start with initial guesses of the dimensions parameters and then iterate between performance analysis and dimension modifications to eventually find the right structure dimensions. With the analytical numerical solutions, non-changed parts of the filter, which is made of the large parts of the filter, could be first computed and stored in terms of its analytical solution form. Then the iterative optimization process can be carried out by simply interfacing the analytical solutions and the FDTD model of the varied part of the filter. Because of no need for the repeated simulations of the large part of the filter.

The fourth recommendation is to extend the time reversal method to synthesis of electromagnetic structures with prescribed responses. For instance, one can specify the desired fields at some distance away from an array. By applying the time reversal, we may be able to find the array elements required. One of the application areas is the wireless power transfer systems. Preliminary work was presented in [64]. However, more comprehensive and systematic developments in applications of the time reversal techniques still need to be researched, particularly in improving the power transfer efficiency. In addition, more extensions of the time reversal to other problems need to be done.

BIBLIOGRAPHY

[1] K. Yee, "Numerical solution of initial boundary value problems involving Maxwell's equations in isotropic media," *IEEE Transactions on antennas and propagation,* vol. 14, pp. 302-307, 1966.

[2] A. Taflove, "Application of the finite-difference time-domain method to sinusoidal steady-state electromagnetic-penetration problems," *IEEE Transactions on Electromagnetic Compatibility,* pp. 191-202, 1980.

[3] A. Taflove, "Review of the formulation and applications of the finite-difference time-domain method for numerical modeling of electromagnetic wave interactions with arbitrary structures," *Wave Motion,* vol. 10, pp. 547-582, 1988.

[4] K. L. Shlager and J. B. Schneider, "A survey of the finite-difference time-domain literature," *Advances in Computational Electrodynamics: The Finite-Difference Time-Domain Method,* vol. 1, pp. 1-62, 1998.

[5] A. Tavlove and S. C. Hagness, "Computational Electrodynamics: The Finite-Difference Time-Domain Method Artech House," *Norwood, MA,* 1995.

[6] S. D. Gedney, "Introduction to the finite-difference time-domain (FDTD) method for electromagnetics," *Synthesis Lectures on Computational Electromagnetics,* vol. 6, pp. 1-250, 2011.

[7] R. Courant, K. Friedrichs, and H. Lewy, "Über die partiellen Differenzengleichungen der mathematischen Physik," *Mathematische annalen,* vol. 100, pp. 32-74, 1928.

[8] T. Namiki, "A new FDTD algorithm based on alternating-direction implicit method," *IEEE Transactions on Microwave Theory and Techniques,* vol. 47, pp. 2003-2007, 1999.

[9] T. Namiki, "3-D ADI-FDTD method-unconditionally stable time-domain algorithm for solving full vector Maxwell's equations," *IEEE Transactions on Microwave Theory and Techniques,* vol. 48, pp. 1743-1748, 2000.

[10] F. Zhen, Z. Chen, and J. Zhang, "Toward the development of a three-dimensional unconditionally stable finite-difference time-domain method," *IEEE Transactions on Microwave Theory and Techniques,* vol. 48, pp. 1550-1558, 2000.

[11] S. Wang, F. L. Teixeira, and J. Chen, "An iterative ADI-FDTD with reduced splitting error," *IEEE microwave and wireless components letters,* vol. 15, pp. 92-94, 2005.

[12] Z. Z. Chen and J. Z. Zhang, "An unconditionally stable 3-D ADI-MRTD method free of the CFL stability condition," *Ieee Microwave and Wireless Components Letters,* vol. 11, pp. 349-351, Aug 2001.

[13] I. Ahmed, E.-K. Chua, E.-P. Li, and Z. Chen, "Development of the three-dimensional unconditionally stable LOD-FDTD method," *IEEE Transactions on antennas and propagation,* vol. 56, pp. 3596-3600, 2008.

[14] Q.-F. Liu, Z. Chen, and W.-Y. Yin, "An arbitrary-order LOD-FDTD method and its stability and numerical dispersion," *IEEE Transactions on Antennas and Propagation,* vol. 57, pp. 2409-2417, 2009.

[15] E. L. Tan, "Unconditionally Stable LOD–FDTD Method for 3-D Maxwell's Equations," *IEEE Microwave and Wireless Components Letters,* vol. 17, pp. 85-87, 2007.

[16] Y.-D. Kong and Q.-X. Chu, "Development of the nearly PML for four-stages split-step unconditionally-stable FDTD method," in *Microwave Conference Proceedings (APMC), 2010 Asia-Pacific*, 2010, pp. 2168-2171.

[17] D. Y. Heh and E. L. Tan, "Further Reinterpretation of Multi-Stage Implicit FDTD Schemes," *IEEE Transactions on Antennas and Propagation,* vol. 62, pp. 4407-4411, 2014.

[18] C. Sun and C. Trueman, "Unconditionally stable Crank-Nicolson scheme for solving two-dimensional Maxwell's equations," *Electronics Letters,* vol. 39, pp. 595-597, 2003.

[19] G. Sun and C. Trueman, "Unconditionally-stable FDTD method based on Crank-Nicolson scheme for solving three-dimensional Maxwell equations," *Electronics Letters,* vol. 40, pp. 589-590, 2004.

[20] G. Sun and C. W. Trueman, "Efficient implementations of the Crank-Nicolson scheme for the finite-difference time-domain method," *IEEE transactions on microwave theory and techniques,* vol. 54, pp. 2275-2284, 2006.

[21] K. Xu, Z. Fan, D.-Z. Ding, and R.-S. Chen, "GPU accelerated unconditionally stable Crank-Nicolson FDTD method for the analysis of three-dimensional microwave circuits," *Progress In Electromagnetics Research,* vol. 102, pp. 381-395, 2010.

[22] L. C. Ma and R. Mittra, "Parallel Implementation of the Periodic Boundary Condition (PBC) in the FDTD for the Investigation of Spatial Filters," *2008 Ieee Antennas and Propagation Society International Symposium, Vols 1-9,* pp. 2626-2629, 2008.

[23] Y. Miyazaki and K. Kouno, "FDTD Analysis of Spatial Filtering of Scattered Waves for Optical CT of Medical Diagnosis," *Piers 2009 Beijing: Progess in Electromagnetics Research Symposium, Proceedings I and Ii,* pp. 1567-1572, 2009.

[24] C. D. Sarris, "Extending the Stability Limit of the FDTD Method With Spatial Filtering," *Ieee Microwave and Wireless Components Letters,* vol. 21, pp. 176-178, Apr 2011.

[25] G. D. Xie, B. Wu, Z. X. Huang, and X. L. Wu, "The Application of Spatial Filtered FDTD Method in Fine Structures," *2016 Ieee International Conference on Ubiquitous Wireless Broadband (Icuwb2016),* 2016.

[26] M. Gaffar and D. Jiao, "An explicit and unconditionally stable FDTD method for electromagnetic analysis," *IEEE Transactions on Microwave Theory and Techniques,* vol. 62, pp. 2538-2550, 2014.

[27] M. Fink, "Time reversed acoustics," *Physics today,* vol. 50, pp. 34-40, 1997.

[28] M. Fink, D. Cassereau, A. Derode, C. Prada, P. Roux, M. Tanter*, et al.*, "Time-reversed acoustics," *Reports on progress in Physics,* vol. 63, p. 1933, 2000.

[29] G. Lerosey, J. De Rosny, A. Tourin, A. Derode, G. Montaldo, and M. Fink, "Time reversal of electromagnetic waves," *Physical review letters,* vol. 92, p. 193904, 2004.

[30] P. Kosmas and C. M. Rappaport, "Time reversal with the FDTD method for microwave breast cancer detection," *IEEE Transactions on Microwave Theory and Techniques,* vol. 53, pp. 2317-2323, 2005.

[31] M. E. Yavuz and F. L. Teixeira, "A numerical study of time-reversed UWB electromagnetic waves in continuous random media," *IEEE Antennas and Wireless Propagation Letters,* vol. 4, pp. 43-46, 2005.

[32] M. Forest and W. J. Hoefer, "TLM synthesis of microwave structures using time reversal," in *Microwave Symposium Digest, 1992., IEEE MTT-S International*, 1992, pp. 779-782.

[33] W. J. Hoefer, "Computational Time Reversal—A Frontier in Electromagnetic Structure Synthesis and Design," *IEEE Transactions on Microwave Theory and Techniques,* vol. 63, pp. 3-10, 2015.

[34] R. Sorrentino, P. P. So, and W. J. Hoefer, "Numerical microwave synthesis by inversion of the TLM process," in *Microwave Conference, 1991. 21st European*, 1991, pp. 1273-1277.

[35] R. Sorrentino, L. Roselli, and P. Mezzanotte, "Time reversal in finite difference time domain method," *IEEE Microwave and Guided wave letters,* vol. 3, pp. 402-404, 1993.

[36] Z. Z. Chen, W. Fan, and S. C. Yang, "Towards the Wave-equation Based Explicit FDTD Method Without Numerical Instability," *2016 IEEE International Conference on Computational Electromagnetics (Iccem),* 2016.

[37] W. Fan, Z. D. Chen, and S. Yang, "A wave equation based unconditionally stable explicit FDTD method," in *Numerical Electromagnetic and Multiphysics Modeling and Optimization (NEMO), 2015 IEEE MTT-S International Conference on*, 2015, pp. 1-3.

[38] W. Fan, Z. Z. Chen, and S. C. Yang, "On the Analytical Solution of the FDTD Method," *Ieee Transactions on Microwave Theory and Techniques,* vol. 64, pp. 3370-3379, Nov 2016.

[39] M. Q. Zhou, Z. Z. Chen, W. Fan, X. Bo, and W. Wei, "A Subgridding Scheme with the Unconditionally Stable Explicit FDTD Method," *2016 Ieee Mtt-S International Conference on Numerical Electromagnetic and Multiphysics Modeling and Optimization (Nemo),* 2016.

[40] W. Fan and Z. Z. Chen, "A Condition for Multiple Source Reconstructions with the Time-Reversal Methods," *2016 Ieee Mtt-S International Microwave Symposium (Ims),* 2016.

[41] S.-C. Yang, Z. Chen, Y. Yu, and W.-Y. Yin, "An unconditionally stable one-step arbitrary-order leapfrog ADI-FDTD method and its numerical properties," *IEEE transactions on antennas and propagation,* vol. 60, pp. 1995-2003, 2012.

[42] Q. He, D. Chen, and D. Jiao, "An Explicit and Unconditionally Stable Time-Domain Finite-Element Method of Linear Complexity for Electromagnetics-Based Simulation of 3-D Global Interconnect Network," *2011 Ieee 20th Conference on Electrical Performance of Electronic Packaging and Systems (Epeps),* pp. 185-188, 2011.

[43] S.-K. Jeng, "An analytical expression for 3-D dyadic FDTD-compatible Green's function in infinite free space via z-transform and partial difference operators," *IEEE Transactions on Antennas and Propagation,* vol. 59, pp. 1347-1355, 2011.

[44] Z. Z. Chen and P. P. Silvester, "Analytic Solutions for the Finite-Difference Time-Domain and Transmission-Line-Matrix Methods," *Microwave and Optical Technology Letters,* vol. 7, pp. 5-8, Jan 1994.

[45] A. Taflove and S. C. Hagness, "Computational Electrodynamics, The Finite-Difference Time-Domain Method. Boston, Artech House," ed: Inc, 2000.

[46] R. B. Lehoucq and D. C. Sorensen, "Deflation techniques for an implicitly restarted Arnoldi iteration," *SIAM Journal on Matrix Analysis and Applications,* vol. 17, pp. 789-821, 1996.

[47] D. A. Gorodetsky and P. A. Wilsey, "Reduction of FDTD simulation time with modal methods," *PIERS 2006 Cambridge: Progress in Electromagnetics Research Symposium, Proceedings,* pp. 510-513, 2006.

[48] Z. Chen and M. M. Ney, "The method of weighted residuals: A general approach to deriving time-and frequency-domain numerical methods," *IEEE Antennas and Propagation Magazine,* vol. 51, 2009.

[49] Z. Z. Chen, Y. Q. Yu, and M. M. Ney, "The Time-domain Method of Weighted Residuals (MWR): Moving from Grid-based Methods to Node-based Meshless Techniques," *Iceaa: 2009 International Conference on Electromagnetics in Advanced Applications, Vols 1 and 2,* pp. 200-+, 2009.

[50] J. Wang, W.-Y. Yin, P.-G. Liu, and Q.-H. Liu, "High-order interface treatment techniques for modeling curved dielectric objects," *IEEE Transactions on Antennas and Propagation,* vol. 58, pp. 2946-2953, 2010.

[51] X.-P. Liang and K. A. Zaki, "Modeling of cylindrical dielectric resonators in rectangular waveguides and cavities," *IEEE transactions on microwave theory and techniques,* vol. 41, pp. 2174-2181, 1993.

[52] J. P. Berenger, "A perfectly matched layer for free-space simulation in finite-difference computer codes," *Annales Des Telecommunications-Annals of Telecommunications,* vol. 51, pp. 39-46, Jan-Feb 1996.

[53] J. P. Berenger, "Perfectly matched layer for the FDTD solution of wave-structure interaction problems," *IEEE Transactions on Antennas and Propagation,* vol. 44, pp. 110-117, Jan 1996.

[54] J. Douma, E. Niederleithinger, and R. Snieder, "Locating events using time reversal and deconvolution: Experimental application and analysis," *Journal of Nondestructive Evaluation,* vol. 34, pp. 1-9, 2015.

[55] D. G. Albert, L. Liu, and M. L. Moran, "Time reversal processing for source location in an urban environment a," *The Journal of the Acoustical Society of America,* vol. 115, pp. 2596-619, 2005.

[56] W. J. Hoefer, "Time reversal and optimal electromagnetic structure synthesis," in *Electromagnetic Theory (EMTS), 2010 URSI International Symposium on*, 2010, pp. 287-290.

[57] W. J. R. Hoefer and R. Vahldieck, "Final report on the first international workshop on transmission line matrix (TLM) modeling - Theory and applications - 1-3 August, 1995, University of Victoria, Victoria, BC, Canada to the Natural Sciences and Engineering Research Council of Canada - Scholarships and international programs, 350 Albert street Ottawa, Canada K1A 1115," *International Journal of Numerical Modelling-Electronic Networks Devices and Fields,* vol. 9, pp. 167-170, Jan-Apr 1996.

[58] M. Krumpholz and P. Russer, "On the foundation of the transmission line matrix (TLM) method," *Ultra-Wideband, Short-Pulse Electromagnetics 2,* pp. 411-419, 1995.

[59] M. Schmidt, "Least squares optimization with L1-norm regularization," *CS542B Project Report,* pp. 14-18, 2005.

[60] D. L. Donoho, "For most large underdetermined systems of linear equations the minimal " *Communications on pure and applied mathematics,* vol. 59, pp. 797-829, 2006.

[61] M. W. Fakhr, E. S. Youssef, and M. S. El-Mahallawy, "L1-Regularized Least Squares Sparse Extreme Learning Machine for Classification," *2015 International Conference on Information and Communication Technology Research (Ictrc),* pp. 222-225, 2015.

[62] W. J. R. Hoefer, "Tracking Impulsive Sources in Space-Time by TLM Time Reversal," *2016 IEEE MTT-S International Microwave Symposium (Ims),* 2016.

[63] Z. Chen, W. Hoefer, and M. Ney, "A new finite-difference time-domain formulation equivalent to the TLM symmetrical condensed node," in *Microwave Symposium Digest, 1991., IEEE MTT-S International*, 1991, pp. 361-364.

[64] F. Cangialosi, T. Grover, P. Healey, T. Furman, A. Simon, and S. M. Anlage, "Time reversed electromagnetic wave propagation as a novel method of wireless power transfer," in *Wireless Power Transfer Conference (WPTC), 2016 IEEE*, 2016, pp. 1-4.

APPENDIX I Derivation of the Equivalence between the CFL Condition and Maximum Eigenvalue of the FDTD System Matrix

In section II, it is shown that the maximum eigenvalue of system matrix **M** will determine whether the FDTD solution is stable or not. In the following paragraphs, we show that such determination is equivalent to the CFL condition.

Since *M* is the discretized finite-difference form of operator $\Delta t^2(\varepsilon\mu)^{-1}\nabla\times\nabla\times$, it is symmetric, semi-positive definite and sparse [3, 5, 6]. The row (or column) of *M* has many non-zero elements. In the two dimensional case, a row can be written as:

$$\left(...,-\frac{1}{\varepsilon\mu}\frac{\Delta t^2}{\Delta x^2},...-\frac{1}{\varepsilon\mu}\frac{\Delta t^2}{\Delta x^2},...-\frac{1}{\varepsilon\mu}\frac{\Delta t^2}{\Delta y^2},...-\frac{1}{\varepsilon\mu}\frac{\Delta t^2}{\Delta y^2},...\frac{1}{\varepsilon\mu}(\frac{2\Delta t^2}{\Delta x^2}+\frac{2\Delta t^2}{\Delta y^2})...\right) \quad \text{(A.1)}$$

The upper bound of matrix eigenvalues has the following relationship with the matrix elements [19]:

Suppose that matrix **M** has the dimension of $N\times N$. Let

$$R_k=\sum_{l=1}^{N}|\,\mathrm{m}_{kl}\,|\ ,\ C_l=\sum_{k=1}^{N}|\,\mathrm{m}_{kl}\,|\ , \quad \text{(A.2)}$$

$$\begin{aligned} R&=\max R_k\ =\frac{1}{\varepsilon\mu}\left(\frac{4}{\Delta x^2}+\frac{4}{\Delta y^2}\right)\Delta t^2\ ,\\ C&=\max C_l=\frac{1}{\varepsilon\mu}\left(\frac{4}{\Delta x^2}+\frac{4}{\Delta y^2}\right)\Delta t^2\ , \end{aligned} \quad \text{(A.3)}$$

where m_{kl} is the element of **M** at the *k*th row and *l*th column. Then the following inequality holds for all the eigenvalues of M:

$$|\,\lambda(\mathbf{M})\,|\le\min(R,C) \quad \text{(A.4)}$$

In section II, we have shown that $\lambda_i<4$ presents the stable solutions. Therefore,

$$\frac{1}{\varepsilon\mu}\left(\frac{4\Delta t^2}{\Delta x^2}+\frac{4\Delta t^2}{\Delta y^2}\right)<=4 \tag{A.5}$$

Or,

$$\Delta t \le \frac{\sqrt{\mu\varepsilon}}{\sqrt{\frac{1}{\Delta x^2}+\frac{1}{\Delta y^2}}} \tag{A.6}$$

This yields the commonly known CFL condition in two dimensions.

By applying the similar process, we can obtain the CFL condition in three dimensions:

$$\Delta t \le \frac{\sqrt{\mu\varepsilon}}{\sqrt{\frac{1}{\Delta x^2}+\frac{1}{\Delta y^2}+\frac{1}{\Delta z^2}}} \tag{A.7}$$

In other words, condition $\lambda_i < 4$ corresponds to the CFL condition.

APPENDIX II Stability Condition of the FDTD Method in Lossy Cases

The purpose of this Appendix is to show that the stability condition developed for lossless cases can be applied to lossy cases. In other words, in a lossy case, $0<\lambda_i<4$ is the necessary condition for stability whereas $\lambda_i > 4$ leads to instability.

In a lossy medium, the wave equation in the Z-domain can be written as (3.23):

$$\left(1+\frac{\sigma\Delta t}{2\varepsilon}\right)zY_i[z]+\left(1-\frac{\sigma\Delta t}{2\varepsilon}\right)z^{-1}Y_i[z]-2Y_i[z]+\lambda_i Y_i[z]=X[z]\ ,$$

$$H_i[z]=\frac{Y_i[z]}{X[z]}=\frac{1}{\left(1+\frac{\sigma\Delta t}{2\varepsilon}\right)}\frac{z}{z^2-\frac{(2-\lambda_i)}{\left(1+\frac{\sigma\Delta t}{2\varepsilon}\right)}z+\frac{\left(1-\frac{\sigma\Delta t}{2\varepsilon}\right)}{\left(1+\frac{\sigma\Delta t}{2\varepsilon}\right)}}\quad . \qquad (A.8)$$

The poles of $H_i[z]$ are the roots of the denominator:

$$z^2-\frac{(2-\lambda_i)}{\left(1+\frac{\sigma\Delta t}{2\varepsilon}\right)}z+\frac{\left(1-\frac{\sigma\Delta t}{2\varepsilon}\right)}{\left(1+\frac{\sigma\Delta t}{2\varepsilon}\right)}=0 \quad . \qquad (A.9)$$

They are

$$z_{i,1or2}=\begin{cases}\dfrac{2-\lambda_i \pm j\sqrt{4\lambda_i-\lambda_i^2-\dfrac{\sigma^2\Delta t^2}{\varepsilon^2}}}{2+\dfrac{\sigma\Delta t}{\varepsilon}} & \text{if} \quad \lambda_i^2-4\lambda_i+\dfrac{\sigma^2\Delta t^2}{\varepsilon^2}<0 \\ \dfrac{2-\lambda_i \pm \sqrt{\lambda_i^2-4\lambda_i+\dfrac{\sigma^2\Delta t^2}{\varepsilon^2}}}{2+\dfrac{\sigma\Delta t}{\varepsilon}} & \text{if} \quad \lambda_i^2-4\lambda_i+\dfrac{\sigma^2\Delta t^2}{\varepsilon^2}>0\end{cases} \qquad (A.10)$$

Now consider the different situations.

Situation 1: $\lambda_i > 4$

In this case, $\lambda_i^2 - 4\lambda_i + \frac{\sigma^2\Delta t^2}{\varepsilon^2} > \frac{\sigma^2\Delta t^2}{\varepsilon^2} > 0$,

$$\max(|z_{i,1}|,|z_{i,2}|) = \left| \frac{2 - \lambda_i - \sqrt{\lambda_i^2 - 4\lambda_i + \frac{\sigma^2\Delta t^2}{\varepsilon^2}}}{2 + \frac{\sigma\Delta t}{\varepsilon}} \right|$$

$$= \frac{\lambda_i - 2 + \sqrt{\lambda_i^2 - 4\lambda_i + \frac{\sigma^2\Delta t^2}{\varepsilon^2}}}{2 + \frac{\sigma\Delta t}{\varepsilon}} \quad , \tag{A.11}$$

Since $\lambda_i - 2 > 2$ and $\sqrt{\lambda_i^2 - 4\lambda_i + \frac{\sigma^2\Delta t^2}{\varepsilon^2}} > \frac{\sigma\Delta t}{\varepsilon} > 0$,

$$\frac{\lambda_i - 2 + \sqrt{\lambda_i^2 - 4\lambda_i + \frac{\sigma^2\Delta t^2}{\varepsilon^2}}}{2 + \frac{\sigma\Delta t}{\varepsilon}} > 1 \tag{A.12}$$

This means that there must be at least one pole lying outside the unit circle. The FDTD solution is then unstable.

Situation 2: $0 < \lambda_i < 4$

In this case, $\lambda_i^2 - 4\lambda_i + \frac{\sigma^2\Delta t^2}{\varepsilon^2}$ could be larger or smaller than zero. The discussions have to be separated in two scenarios.

If $0 < \lambda_i < 4$, we will have $\lambda_i^2 - 4\lambda_i + \frac{\sigma^2\Delta t^2}{\varepsilon^2} < 0$.

$$\left|z_{i,1}\right|=\left|z_{i,2}\right|=\frac{\sqrt{(2-\lambda_i)^2+4\lambda_i-\lambda_i{}^2-\dfrac{\sigma^2\Delta t^2}{\varepsilon^2}}}{2+\dfrac{\sigma\Delta t}{\varepsilon}}$$

$$=\frac{\sqrt{4-\dfrac{\sigma^2\Delta t^2}{\varepsilon^2}}}{2+\dfrac{\sigma\Delta t}{\varepsilon}}<1 \quad . \qquad \text{(A.13)}$$

If $0<\lambda_i<4$ and $\lambda_i{}^2-4\lambda_i+\dfrac{\sigma^2\Delta t^2}{\varepsilon^2}>0$,

Let $f(\lambda_i)=\max(\left|z_{i,1}\right|,\left|z_{i,2}\right|)=\max(\left|\dfrac{2-\lambda_i\pm\sqrt{\lambda_i{}^2-4\lambda_i+\dfrac{\sigma^2\Delta t^2}{\varepsilon^2}}}{2+\dfrac{\sigma\Delta t}{\varepsilon}}\right|)$, then

$$f(\lambda_i,4>\lambda_i>2)=\left|\frac{2-\lambda_i-\sqrt{\lambda_i{}^2-4\lambda_i+\dfrac{\sigma^2\Delta t^2}{\varepsilon^2}}}{2+\dfrac{\sigma\Delta t}{\varepsilon}}\right|$$

$$=\frac{\lambda_i-2+\sqrt{\lambda_i{}^2-4\lambda_i+\dfrac{\sigma^2\Delta t^2}{\varepsilon^2}}}{2+\dfrac{\sigma\Delta t}{\varepsilon}} \qquad \text{(A.14)}$$

$$f(\lambda_i, 2 \geq \lambda_i > 0) = \left| \frac{2 - \lambda_i + \sqrt{\lambda_i^2 - 4\lambda_i + \frac{\sigma^2 \Delta t^2}{\varepsilon^2}}}{2 + \frac{\sigma \Delta t}{\varepsilon}} \right|$$

$$= \frac{2 - \lambda_i + \sqrt{\lambda_i^2 - 4\lambda_i + \frac{\sigma^2 \Delta t^2}{\varepsilon^2}}}{2 + \frac{\sigma \Delta t}{\varepsilon}} \qquad \text{(A.15)}$$

Since $\lambda_i - 2 < 2$, $0 < \sqrt{\lambda_i^2 - 4\lambda_i + \frac{\sigma^2 \Delta t^2}{\varepsilon^2}} < \frac{\sigma \Delta t}{\varepsilon}$, $f(\lambda_i, 4 > \lambda_i > 2) < 1$.

Since $2 - \lambda_i \leq 2$, $0 < \sqrt{\lambda_i^2 - 4\lambda_i + \frac{\sigma^2 \Delta t^2}{\varepsilon^2}} < \frac{\sigma \Delta t}{\varepsilon}$, $f(\lambda_i, 2 \geq \lambda_i > 0) < 1$

In summary, we show that when $0 < \lambda_i < 4$, the FDTD solution itself is stable and when $\lambda_i > 4$, the FDTD solutions are unstable. The condition applies to both lossless and lossy cases. The difference is that when $0 < \lambda_i < 4$ is satisfied, the poles of the system matrix lie on the unit circle in a lossless case but inside of the unit circle in a lossy case.

APPENDIX III Copyright Permission

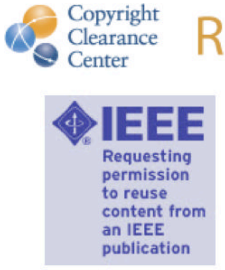

Title: Source Reconstruction From Wideband and Band-Limited Responses by FDTD Time Reversal and Regularized Least Squares
Author: Wei Fan
Publication: Microwave Theory and Techniques, IEEE Transactions on
Publisher: IEEE
Date: Dec. 2017
Copyright © 2017, IEEE

LOGIN
If you're a copyright.com user, you can login to RightsLink using your copyright.com credentials. Already **a RightsLink user** or want to learn more?

Thesis / Dissertation Reuse

The IEEE does not require individuals working on a thesis to obtain a formal reuse license, however, you may print out this statement to be used as a permission grant:

Requirements to be followed when using any portion (e.g., figure, graph, table, or textual material) of an IEEE copyrighted paper in a thesis:

1) In the case of textual material (e.g., using short quotes or referring to the work within these papers) users must give full credit to the original source (author, paper, publication) followed by the IEEE copyright line © 2011 IEEE.
2) In the case of illustrations or tabular material, we require that the copyright line © [Year of original publication] IEEE appear prominently with each reprinted figure and/or table.
3) If a substantial portion of the original paper is to be used, and if you are not the senior author, also obtain the senior author's approval.

Requirements to be followed when using an entire IEEE copyrighted paper in a thesis:

1) The following IEEE copyright/ credit notice should be placed prominently in the references: © [year of original publication] IEEE. Reprinted, with permission, from [author names, paper title, IEEE publication title, and month/year of publication]
2) Only the accepted version of an IEEE copyrighted paper can be used when posting the paper or your thesis on-line.
3) In placing the thesis on the author's university website, please display the following message in a prominent place on the website: In reference to IEEE copyrighted material which is used with permission in this thesis, the IEEE does not endorse any of [university/educational entity's name goes here]'s products or services. Internal or personal use of this material is permitted. If interested in reprinting/republishing IEEE copyrighted material for advertising or promotional purposes or for creating new collective works for resale or redistribution, please go to http://www.ieee.org/publications_standards/publications/rights/rights_link.html to learn how to obtain a License from RightsLink.

If applicable, University Microfilms and/or ProQuest Library, or the Archives of Canada may supply single copies of the dissertation.

BACK CLOSE WINDOW